SEARCH FOR THE SM AND MSSM HIGGS BOSON IN THE $t\bar{t}H, H \to b\bar{b}$ CHANNEL*

Elżbieta Richter-Wąs

CERN, IT Division, 1211 Geneva 23, Switzerland
Institute of Computer Science, Jagellonian University
Nawojki 11, 30-072 Cracow, Poland
Institute of Nuclear Physics
Kawiory 26a, 30-055 Cracow, Poland

and Mariusz Sapiński

Institute of Nuclear Physics
Kawiory 26a, 30-055 Cracow, Poland

(Received December 18, 1998)

A detailed study of the associated Standard Model Higgs boson production $t\bar{t}H$ with $H \to b\bar{b}$ is presented for the SM and MSSM scenarios. For Higgs boson masses from 80 to 120 GeV and an integrated luminosity of $3 \cdot 10^4$ pb^{-1} a clear evidence for an excess of events with four b-tagged jets over the background from $W +$ jets and $t\bar{t}$ production should be observable. However, a clean reconstruction of the $H \to b\bar{b}$ mass peak will be difficult because of the combinatorial background from the signal itself. This problem can be to a large extent overcome if both top-quark decays are reconstructed in addition to the reconstruction of the $H \to b\bar{b}$ mass peak. In the MSSM scenario, the low $\tan\beta$ region (up to $\tan\beta \sim 6$) for an integrated luminosity of $3 \cdot 10^4$ pb^{-1} and most of the $(m_A, \tan\beta)$ parameter space for an integrated luminosity of 10^5 pb^{-1} would be accessible with this channel. Excellent b-tagging capability and good efficiency for jet reconstruction are however necessary to explore this channel to its full potential.

PACS numbers: 14.80.Bn, 14.80.Cp, 14.65.Ha

* Supported in part by Polish Government grant 2P03B00212, 115/E-343/SUPB/P03/004/97, 115/E-343/SPUB/P03/157/98 and Polish-American Maria Skłodowska-Curie Joint Fund II in cooperation with PAA and DOE under project PAA/DOE-97-316.

1. Introduction

The $t\bar{t}H, H \to b\bar{b}$ channel has been proposed [1,2] as an interesting channel to search for the SM and MSSM Higgs.

The final state of this channel is rather complex. One top decay, $t \to Wb$, is required to be followed by the semileptonic decay of the W-boson, $W \to \ell\nu$, to provide an isolated lepton for the trigger. This provides a final state topology with one isolated lepton and at least four reconstructed jets originating from the b-quarks or hadronic decay of the second W-boson. Either four or three of these reconstructed jets are required to be identified as b-jets by the selection procedure. The Higgs signal would thus appear as a peak in the invariant $b\bar{b}$ mass distribution, above the combinatorial background from the signal itself and from the various background processes, which can be divided into two categories:

- the irreducible background, consisting of the resonant $t\bar{t}Z$ channel with $Z \to b\bar{b}$ decay and of $t\bar{t}b\bar{b}$ production;
- the reducible backgrounds containing jets misidentified as b-jets, such as $t\bar{t}jj$, $Wjjj$, $Wjbb$ *etc.* Their magnitude will obviously depend on the quality of the b-tagging performance.

A careful evaluation of the potential in this channel with $3b$-tagged jets in the final state was performed in [2]. The main results from this paper are briefly recalled below.

- For $m_H = 100$ GeV, 20% of the events contain two (reconstructed) b-jets, 44% contain three b-jets and 32% contain four b-jets. However, only 39% of all reconstructed b-jets come from $H \to b\bar{b}$ decay, whereas 61% come from top quark decay. This indicates that the combinatorial background itself will be quite large when searching for a peak in the invariant mass of two tagged b-jets.
- The largest of all background sources is that from $t\bar{t}$ + jets, both in the case of three and four b-tagged jets, provided the rejection against light-quark and gluon jets can be kept at the level of $R_{\mathrm{jet}} = 50$ or more.
- For events with three b-tagged jets, the obvious but naive method, which includes all three mass combinations in the m_{bb} distribution, each one with a weight of 1/3, leads to only 30% of the total event rate observed in the mass window, $60 < m_H < 100$ GeV, containing a $b\bar{b}$ pair from Higgs decay.

- Variations of this method, *e.g.* (a) choosing only combinations containing the b-jet with lowest p_{T} (since the b-jets from $H \to b\bar{b}$ decays tend to have lower p_{T} than those from top quark decay) or (b) weighting each combination with $1/N$, where N is the number of combinations falling in the mass window for the event considered, lead finally only to small increases of the fraction of true $H \to b\bar{b}$ combinations inside the mass window (never more than 40%).

- For an integrated luminosity of $3 \cdot 10^4$ pb^{-1} in ATLAS and different assumptions on the b-tagging efficiency ($\varepsilon_b = 0.3,\ 0.5,\ 0.7$ with respectively R_{jet} =100, 50, 10), the expected significance (S/$\sqrt{\mathrm{B}}$) does not exceed 3σ a value too small to claim discovery in this channel alone.

- The identification of all four b-jets is very expensive in terms of signal rate and therefore requires excellent b-tagging performance.

The $t\bar{t}H, H \to b\bar{b}$ channel is the only one which does not have to contend with potentially dangerous background from the Z-resonance, owing to the very small value of the $t\bar{t}Z, Z \to b\bar{b}$ cross-section with respect to the signal one. On the other hand, it is plagued by the combinatorial background from the large multiplicity of b-jets present in the final state.

This paper discusses the observability of the $t\bar{t}H$, $H \to b\bar{b}$ channel with four b-tagged jets. Although the identification of four b-jets is very expensive in terms of signal rate, a more complete reconstruction of the final state is possible in this case and, hence, the suppression of the combinatorial background. The key to suppress the combinatorial background, as suggested in [2], is the full reconstruction of the final state, *i.e.* the reconstruction of both top-quark decays as well as that of the $H \to b\bar{b}$ decay.

This paper is organised as follows. Section 1 briefly discusses the results of various inclusive selection procedures for extracting a SM $H \to b\bar{b}$ signal in the case of 4 b-tagged jets. Section 2 describes the top-quark decay reconstruction procedure with emphasis on the quality criteria used for the reconstruction. Section 3 presents the final results for the SM $t\bar{t}H$ channel with full reconstruction of the final state. Section 4 extends these results to the case of the light Higgs boson, h, in the MSSM model, and, finally, Section 5 presents the conclusions.

2. Observability of the $t\bar{t}H$, $H \to b\bar{b}$ channel with four b-tagged jets

Signal and background events are generated using the PYTHIA 5.7 Monte Carlo package [6]. Since the exact calculations for the multi-jet background final states are not available, the parton shower approximation has to be used to simulate the $t\bar{t}$+jets and W+jets backgrounds. This approximation tends to underestimate these backgrounds as has been shown in [3,4], and uncertainties in the background predictions could therefore be as large as a factor of 2. Nevertheless, the background generation is performed as much as possible in an unbiased way, generating the $t\bar{t}$ and W + jet hard-scattering processes in several $p_{\rm T}^{\rm hard}$ bins, starting from $p_{\rm T}^{\rm hard} > 1$ GeV. Table I gives the cross-sections for the signal and background processes as a function of m_H and $p_{\rm T}^{\rm hard}$.

TABLE I

Production cross-sections for the signal and background processes. The branching ratio for one semileptonic $W \to \ell\nu$ decay ($\ell = e, \mu$) and for $H \to b\bar{b}$, $Z \to b\bar{b}$ are included.

Process	σ [pb]	Process	σ [pb]
$t\bar{t}H$			
m_H=80 GeV	0.730		
m_H=100 GeV	0.390	$t\bar{t}Z$	0.033
m_H=120 GeV	0.200		
$t\bar{t}$+ jets		W+jets	
$p_{\rm T}^{\rm hard} = 1-20$ GeV	5.8	$p_{\rm T}^{\rm hard} = 1-20$ GeV	57400
$p_{\rm T}^{\rm hard} = 20-50$ GeV	27.7	$p_{\rm T}^{\rm hard} = 20-50$ GeV	5950
$p_{\rm T}^{\rm hard} = 50-100$ GeV	71.0	$p_{\rm T}^{\rm hard} = 50-100$ GeV	1540
$p_{\rm T}^{\rm hard} = 100-200$ GeV	93.1	$p_{\rm T}^{\rm hard} = 100-150$ GeV	255
$p_{\rm T}^{\rm hard} > 200$ GeV	33.8	$p_{\rm T}^{\rm hard} = 150-200$ GeV	53.3
		$p_{\rm T}^{\rm hard} = 200-300$ GeV	28.0
		$p_{\rm T}^{\rm hard} > 300$ GeV	7.2

For the analysis presented in this note, the generated signal and background events are passed through the fast simulation of the ATLAS detector [5] in the following way:

- the fast simulation package ATLFAST reconstructs jets and isolated leptons with the energy resolutions and acceptances expected for ATLAS. Jets are reconstructed by default for $p_{\rm T} > 15$ GeV (before rescaling to the original parton energy) and $|\eta| <5.0$, whereas isolated leptons are reconstructed for $p_{\rm T} > 6$ GeV and $|\eta| < 2.5$. Hadronic jets are labelled as true b-jets or c-jets if they are within the b-tagging acceptance of the Inner Detector, $|\eta| < 2.5$, and if they are associated to a parent c-quark or b-quark, with $p_{\rm T} > 5$ GeV;

- the overall ATLAS b-tagging performance is emulated in an approximate manner by randomly tagging true b-jets as such with a probability of 60% (resp. 50%) at low (resp. high) luminosity, by randomly mis-tagging true c-jets as b-jets with a probability of 10%, and by randomly mis-tagging all other jets as b-jets with a probability of 1%.

- jet energies are rescaled on average to the original parton energies using p_{T}-dependent scaling factors determined separately for b-jets and non-b-jets. After this procedure has been applied, the peak positions for the invariant mass distributions for $b\bar{b}$ pairs from $H \to b\bar{b}$ decays and jj pairs from $W \to jj$ decays are at the correct values within $\pm 1\%$. The degradation of the jet energy resolution due to pile-up at high luminosity is included in a rather crude manner (a contribution with r.m.s of 7.5 GeV in E_{T} is added to the resolution), so the results shown below for the reconstruction of the $H \to b\bar{b}$ peak should be considered as optimistic.

After initial selection, several algorithms to suppress the combinatorial background to the m_{bb} distribution are studied and compared:

- the so-called "naive" selection, where all possible combinations of b-jet pairs out of 4 b-tagged jets contribute to the m_{bb} mass distribution (six possible combinations);
- the so-called "three + one" selection, which chooses only the b-jet pairs from the set of the three closest jets, leaving out (as candidate for $t \to Wb$ decay) the furthest one (three possible combinations);
- the so called "top-rec" selection, which selects the b-jet, which gives the best value of $\chi^2 = (m_{\ell\nu b} - m_t)^2$ as coming from $t \to Wb$ decay. Any combination of the remaining three b-jets contributes to the m_{bb} distribution (three possible combinations).
- the so called "top-rec with cut" selection, which starts with the top-quark reconstruction in the $t \to \ell\nu b$ decay requires the mass of the reconstructed $t \to \ell\nu b$ decay to be within a window $m_{\ell\nu b} = 175 \pm 30$ GeV. This reconstruction selects one b-jet out of four. Any combination of the remaining three b-jets contributes to the m_{bb} distribution (three possible combinations).

For the signal events the efficiency of the preliminary selection, requiring at least 4 reconstructed jets within $|\eta| < 5.0$ and one isolated lepton, is 74%. Requiring in addition 4 b-tagged jets reduces the acceptance to 5.3% for the expected low-luminosity b-tagging performance ($\varepsilon_b = 60\%$). The relative efficiencies of the additional selection algorithms described above are, respectively, 100% for the "naive", "three+one" and "top-rec" selection and 72% for the "top-rec with cut" selection. The acceptance of the mass window cut itself, $m_{bb} = m_H \pm 2\sigma_{m_{bb}}$, varies between 50 and 70%. The total acceptance thus varies between 1.5 and 2.0%. The mass resolutions and the expected numbers of events accepted in the mass windows for the different algorithms are summarised in Table II.

For the algorithms described above Fig. 1 shows the m_{bb} distribution for the signal events and its content in true $H \to b\bar{b}$ combinations; the combinatorial background from the signal events themselves is significant in all cases.

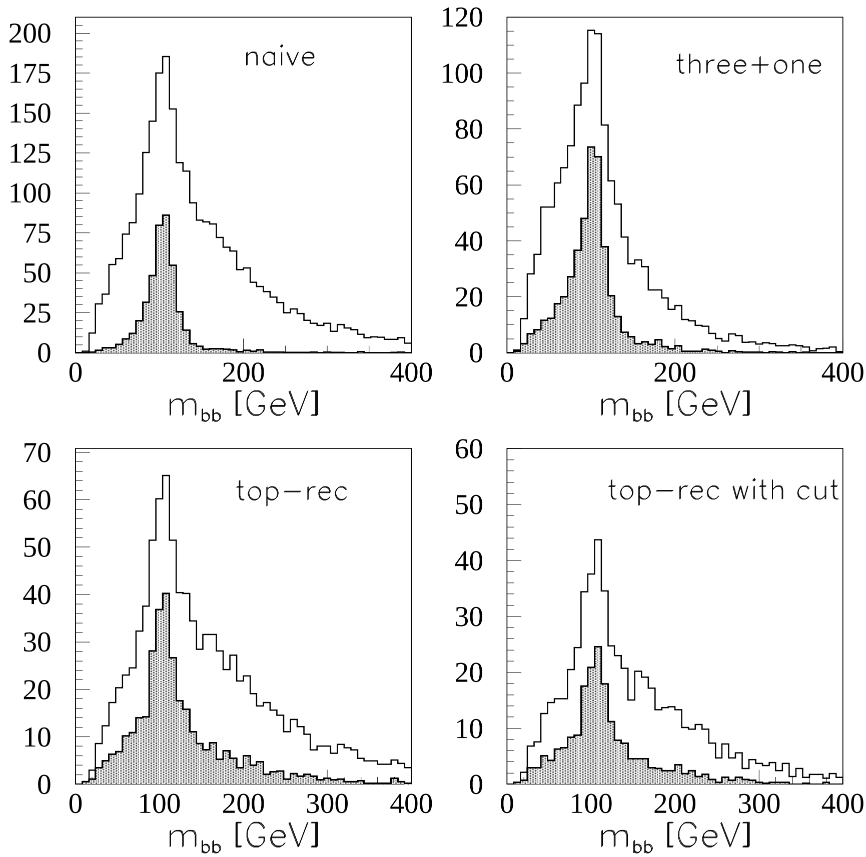

Fig. 1. Distribution of invariant mass, m_{bb}, of b-jet pairs (white histogram) for $t\bar{t}H$, $H \to b\bar{b}$ signal events reconstructed using the "naive", "three+one", "top-rec" and "top-rec with cut" algorithms (see text) for an integrated luminosity of $3 \cdot 10^4$ pb^{-1}. The true $H \to b\bar{b}$ combinations are also shown (shaded histogram). For "naive" method six and otherwise three combinations per event enter the plot.

TABLE II

Expected mass resolution, $\sigma_{m_{b\bar{b}}}$ and numbers of events within the mass windows for an integrated luminosity of $3 \cdot 10^4$ pb^{-1} and for $t\bar{t}H$, $H \to b\bar{b}$ signal events with m_H=100 GeV reconstructed using the algorithms described in the text.

	$\sigma_{m_{bb}}$	Events within		Fraction of $H \to b\bar{b}$ within	
Algorithm	(GeV)	$\pm 2\sigma_{m_{bb}}$	± 20 GeV	$\pm 2\sigma_{m_{bb}}$	± 20 GeV
"naive"	20	206	125	28%	40%
"three+one"	24	209	112	33%	51%
"top-rec"	20	237	117	28%	43%
"top-rec with cut"	20	154	86	30%	44%

The requirement of four b-tagged jets strongly suppresses the W+jets background. Although its initial cross-section is several orders of magnitude larger than that of for the $t\bar{t}$+jets process, after the selection procedure, it contributes only at the level of 5% of the total background. Table III shows the expected numbers of signal and background events as a function of the sequential steps taken in the "naive" reconstruction algorithm.

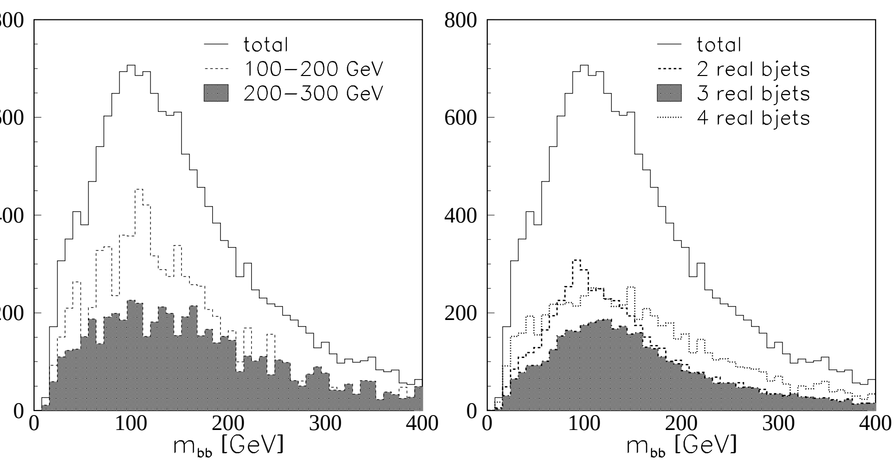

Fig. 2. Total expected background from $t\bar{t}$+ jets events (solid histogram) in the m_{bb} distribution reconstructed using the "naive" algorithm (see text), for an integrated luminosity of $3 \cdot 10^4$ pb^{-1}. The lefthand plot illustrates contributions from different $p_{\rm T}^{\rm hard}$ bins and the righthand plot those from events containing two, three or four true b-jets in the final state.

Fig. 2 shows the m_{bb} distribution obtained for the $t\bar{t}$+jets background using the "naive" reconstruction algorithm. Separately shown are the contributions from different $p_{\rm T}^{\rm hard}$ bins (lefthand plots) and from the different multiplicities of true b-jets in the events (righthand plots). The $t\bar{t}$+jets background is dominated by $t\bar{t}b\bar{b}$ and $t\bar{t}$jj events. Clearly there is a need for a matrix element calculation of $t\bar{t}b\bar{b}$ final states to check whether PYTHIA 5.7 correctly generates the ratio of $t\bar{t}jj$ to $t\bar{t}b\bar{b}$ events. A matrix element calculation of $t\bar{t}jj$ final states would be also extremely useful to better evaluate the uncertainties in the background estimates presented here.

TABLE III

Expected numbers of signal (m_H=100 GeV) and background events for an integrated luminosity of $3 \cdot 10^4$ pb^{-1} as a function of the sequential steps taken in the "naive" reconstruction algorithm (see text).

Process	One isol. lepton + 4 jets in $\lvert\eta\rvert < 5.0$	$4b$-tagged jets	m_{bb} in $\pm 2\sigma_{m_{bb}}$ mass window	Total acceptance
$t\bar{t}H$	7953	440	206	1.8 %
$t\bar{t}Z$	800	50	15	1.5 %
$t\bar{t}$ + jets in $p_{\rm T}^{\rm hard}$ bins				
1–20 GeV	$6.0 \cdot 10^4$	40	20	$3.3 \cdot 10^{-4}$
20–50 GeV	$3.0 \cdot 10^5$	200	100	$3.3 \cdot 10^{-4}$
50–100 GeV	$8.3 \cdot 10^5$	670	300	$3.6 \cdot 10^{-4}$
100–200 GeV	$1.4 \cdot 10^6$	4200	450	$3.2 \cdot 10^{-4}$
> 200 GeV	$4.8 \cdot 10^5$	670	200	$4.2 \cdot 10^{-4}$
Total ($t\bar{t}$ + jets)	$2.8 \cdot 10^6$	2740	1040	$3.6 \cdot 10^{-4}$
W + jets in $p_{\rm T}^{\rm hard}$ bins				
1–20 GeV	$4.7 \cdot 10^6$	27	11	$2.3 \cdot 10^{-6}$
20–50 GeV	$2.7 \cdot 10^6$	16	7	$2.6 \cdot 10^{-6}$
50–100 GeV	$2.1 \cdot 10^6$	12	5	$2.4 \cdot 10^{-6}$
100–150 GeV	$0.7 \cdot 10^6$	9	3	$2.1 \cdot 10^{-5}$
150–200 GeV	$0.28 \cdot 10^6$	4	2	$1.7 \cdot 10^{-5}$
200–300 GeV	$0.17 \cdot 10^6$	3	1	$3 \cdot 10^{-5}$
> 300 GeV	$0.06 \cdot 10^6$	3	1	$3 \cdot 10^{-5}$
Total (W + jets)	$10 \cdot 10^6$	74	30	$4.8 \cdot 10^{-6}$

Tables IV and V give the expected numbers of signal and background events for an integrated luminosity of $3 \cdot 10^4$ pb^{-1}. The signal–to–background ratio is around 16–19% and the purity of the $H \to b\bar{b}$ signal itself[1] ($S_{H\to b\bar{b}}/S_{\rm total}$) is 28–45%, depending on the mass window and selection algorithm used. The narrow mass window (Table V) gives better signal purities ($S_{H\to b\bar{b}}/S_{\rm total}$) while the wider one (Table IV) gives better significances for the same signal–to–background ratio. However, for all the algorithms described above, the m_{bb} distribution is very similar in shape for the signal and the background and peaks around $m_{bb} = 100$GeV, as shown in Fig. 3. For the background this shape is caused by the effect of the kinematical requirements (4 jets reconstructed with $p_{\rm T} > 15$ GeV). Although significances above 5σ can be reached on paper for an integrated luminosity of $3 \cdot 10^4$ pb^{-1} clearly a very good knowledge of the overall normalisation and shape of the background would be required to claim a firm discovery in this channel using one of the selection algorithms discussed above.

TABLE IV

Expected numbers of Signal (S) and Background (B) events, signal-to-background ratios and significances for an integrated luminosity of $3 \cdot 10^4$ pb^{-1}, for m_H= 100 GeV and for a mass window $m_H \pm 2\sigma_{m_{b\bar{b}}}$.

Process	naive	three+one	top-rec	top-rec with cut
$t\bar{t}H$ (total S)	206	194	237	154
$t\bar{t}Z$	15	10	7	6
$t\bar{t}jj$	1040	1000	1410	940
$Wjjjj$	30	20	30	8
Total B	1085	1030	1447	954
S/B	0.19	0.19	0.16	0.16
S/$\sqrt{\rm B}$	6.3	6.0	6.2	5.0
S$_{H\to b\bar{b}}$/S$_{\rm total}$	28%	37%	28 %	30%

[1] Considered as true $H \to b\bar{b}$ combinations are those where both b-tagged jets are within a distance $\Delta R^{b,b-{\rm rec}} < 1.0$ from the original b-quarks from the Higgs-boson decay.

TABLE V

Same as Table IV for a mass window $m_H \pm 20$ GeV

Process	naive	three+one	top-rec	top-rec with cut
$t\bar{t}H$ (total S)	125	144	117	86
$t\bar{t}Z$	10	11	6	6
$t\bar{t}jj$	740	780	720	580
$Wjjjj$	15	15	17	4
Total B	765	806	743	590
S/B	0.16	0.18	0.16	0.14
$\mathrm{S}/\sqrt{\mathrm{B}}$	4.5	5.1	4.3	3.5
$\mathrm{S}_{H\to b\bar{b}}/\mathrm{S}_{\mathrm{total}}$	40%	45%	43 %	44%

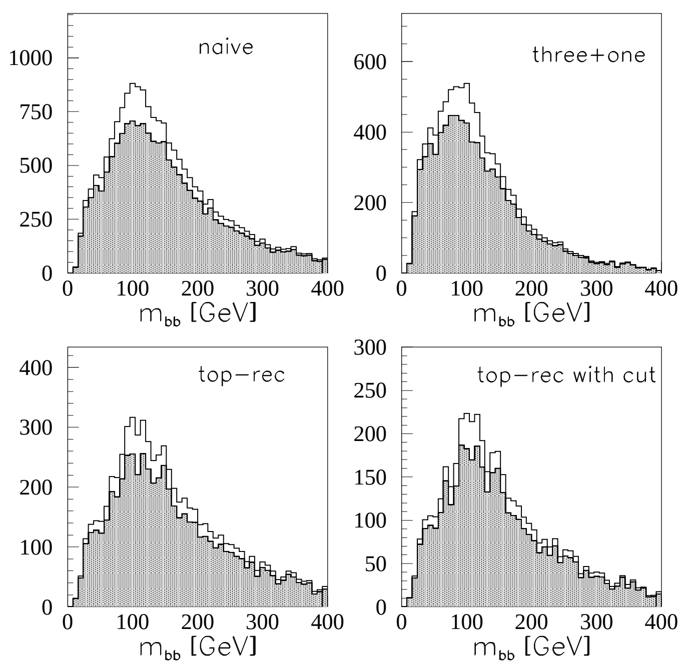

Fig. 3. Distribution of $m_{b\bar{b}}$ for the summed signal + background (solid histogram) and for the background alone (shaded histogram) for different selection algorithms (see text). The results are shown for an integrated luminosity of $3 \cdot 10^4$ pb^{-1}.

3. Top-quark reconstruction with perfect b-tagging

As already mentioned, the full reconstruction of the final state should help to suppress the large combinatorial backgrounds discussed in Section 2 as well as to modify the shape of the $t\bar{t}jj$ background. This section discusses the single and double top-quark reconstruction, as could be expected in the ATLAS detector for inclusive $t\bar{t}$ events.

The initial selection requires at least 4 reconstructed jets with $p_{\mathrm{T}} > 15$ GeV and $|\eta| < 2.5$, two of them being labelled as b-jet and at least one reconstructed isolated lepton ($|\eta| < 2.5$ and $p_{\mathrm{T}}^{\mu} > 6$ GeV or $p_{\mathrm{T}}^{e} > 20$ GeV). The total acceptance of this selection for inclusive $t\bar{t}$ events with one $W \to \ell\nu$ decay is about 33 %. These events become top-pair candidates after passing through the reconstruction algorithm described below[2].

3.1. Single top-quark reconstruction in the semileptonic channel

3.1.1. $W \to \ell\nu$ reconstruction

As is well known a complete reconstruction of $W \to \ell\nu$ decays is limited by the impossibility of reconstructing fully the neutrino four-momentum. The transverse components of the neutrino momentum are assumed to be equal to the corresponding components of the missing energy in the event, while the information on the longitudinal component is lost because of the large amount of energy escaping down the beampipe. This information can be recovered by solving the equation for the mass of the W-boson, which requires the reconstructed neutrino and lepton system to form the W-mass. From this equation:

$$m_W^2 = (E^{\nu} + E^{\ell})^2 - (p_x^{\nu} + p_x^{\ell})^2 - (p_y^{\nu} + p_y^{\ell}) - (p_z^{\nu} + p_z^{\ell})^2 \,, \qquad (1)$$

where $p_x^{\nu} = p_x^{\mathrm{miss}}$, $p_y^{\nu} = p_x^{\mathrm{miss}}$ and the neutrino is assumed massless, the component p_z^{ν} can be extracted. For the cases where there are one or two possible solutions of the above equation, the event is reconstructed further, otherwise it is rejected. The impact of the natural width of the W-boson has to be ignored in this approach.

The quality of the $W \to \ell\nu$ reconstruction is most of all affected by the experimental resolution on the reconstruction of the neutrino four-momentum. Fig. 4 shows the quality of the p_z^{ν} and p_x^{ν} reconstruction as expected for ATLAS using the above procedure for inclusive $t\bar{t}$ events. A resolution of $\sigma_{\nu} = 10.9$ GeV is obtained for the p_x^{ν} reconstruction. The Gaussian part of the p_z^{ν} resolution can be fitted with a resolution $\sigma = 14.3$ GeV, but the

[2] If not specified explicitly in this section, a perfect b-tagging performance is assumed ($\varepsilon_b = 1.0,\ R_c = 10^6,\ R_j = 10^6$)

distribution displays large symmetric tails. The distances between the reconstructed ν and W directions from their true initial directions are also presented in Fig. 4. Only 36% of the events satisfy the condition for a good p_z^ν reconstruction, $|p_z^\nu - p_z^{\nu-\mathrm{rec}}| < 3\sigma$ (whereas 90% of the events do satisfy this condition for p_x^ν reconstruction. Accepting events with an unresolved W-mass equation by assuming $p_z^\nu = 0$ and requiring $m_{\ell\nu} = m_W \pm 5$ GeV increases the acceptance by only 4% but obviously degrades the final resolution on the top-quark mass. The "quality" of the $W \to \ell\nu$ reconstruction is illustrated through the distributions in Fig. 4.

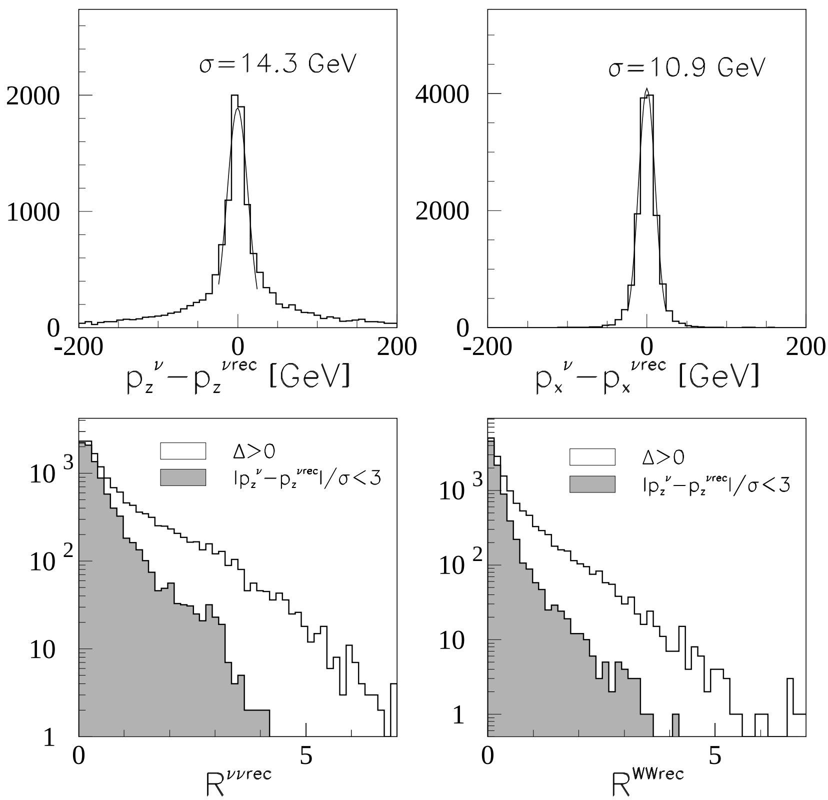

Fig. 4. For $W \to \ell\nu$ decays in inclusive $t\bar{t}$ events, distributions of the difference between reconstructed and initial quantities for the neutrino longitudinal(top left) and transverse (top right) momentum components, and for the directions of the neutrino (bottom left) and W-boson (bottom right). These distributions are shown for events for which equation (1) can be solved (see text), and also for events with $|p_z^\nu - p_z^{\nu-\mathrm{rec}}| < 3\sigma$ (shaded histograms).

3.1.2. $t \to \ell\nu b$ reconstruction

For events containing a reconstructed $W \to \ell\nu$ decay, each of the possible $\ell\nu b$ combinations is considered and the one which best reconstructs the top-quark mass, *i.e.* which minimises the value of $\chi^2 = (m_{\ell\nu b} - m_t)^2$, is chosen as the top-quark candidate.

A complete reconstruction of the $t \to \ell\nu b$ decay requires reconstruction of the $W \to \ell\nu$ decay and of the corresponding b-jets. Both these components contribute significantly to the mass resolution obtained for the top-quark. Table VI shows the resulting resolution σ_m and the fraction of decays with $m_{\ell\nu b}$ outside $\pm 2\sigma_m$ for fully reconstructed $t \to \ell\nu b$ decays and for partially reconstructed $t \to \ell\nu b$ decays, where the reconstructed W or b-jet is replaced by the initial W-boson or b-quark. For the partial reconstruction, the obtained resolutions are respectively $\sigma_m = 8.7$ and 8.3 GeV with 19% and 20 % of the events falling outside the respective $\pm 2\sigma_m$ mass windows. For the full reconstruction, the obtained resolution is $\sigma_m = 10.0$ GeV with 16% of the events falling outside the $\pm 2\sigma_m$ mass window. Fig. 5 shows the resulting $m_{\ell\nu b}$ distributions for the partial and full reconstruction.

Taking as an initial selection for $t \to \ell\nu b$ reconstruction events for which the W-mass equation can be solved one can study possible "quality" cuts for the $t \to \ell\nu b$ reconstruction. Tables VII and VIII show examples of such "quality" cuts using the distances $R^{W,W-\mathrm{rec}}$, $R^{\nu,\nu-\mathrm{rec}}$ and $R^{t,t-\mathrm{rec}}$ between the reconstructed and initial directions of the W-boson, the neutrino and the top-quark, respectively. Although these quantities are not accessible experimentally they can be used to define the fraction of "correct" and "false" top-quark reconstructions. The acceptance (Acc) of such "quality" cuts, the ratio of events passing such "quality" cuts to all events inside the chosen mass window of ± 20 GeV (R_p) and outside this mass window (R_t) and the fraction of events outside the mass window are given in Table VIII. In all cases the fraction of events outside ± 20 GeV is around 15%. The highest quality reconstruction would maximise the value of $Acc \cdot R_p/R_t$; this value is found to be between 0.50 and 0.75 for the "quality" cuts presented in Table VIII. The best reconstruction should also be characterised by a large difference between the values of R_p and R_t; this difference is found to vary between 0.06 and 0.12 for the "quality" cuts presented in Table VIII. The $m_{\ell\nu b}$ distributions before and after "quality" cuts on $R^{W,W-\mathrm{rec}}$, $R^{\nu,\nu-\mathrm{rec}}$, $R^{t,t-\mathrm{rec}}$ are shown in Fig. 6. The acceptance of these "quality" cuts only is between 50 and 80% (see Table VIII), which quantifies the fraction of correctly reconstructed $t \to \ell\nu b$ decays.

TABLE VI

Mass resolutions and fractions of events in tails for fully and partially reconstructed $t \to \ell\nu b$ decays in inclusive $t\bar{t}$ events (see text).

Selection	σ_m [GeV]	Fraction outside $\pm 2\sigma_m$	Fraction outside $\pm 2\sigma_1$
$W^{\rm rec} - b_{\rm jet}$	$10.0 \pm 0.4(\sigma_1)$	16%	16%
$W^{\rm true} - b_{\rm jet}$	8.7 ± 0.3	19%	15%
$W^{\rm rec} - b_{\rm quark}$	8.3 ± 0.3	20%	15%

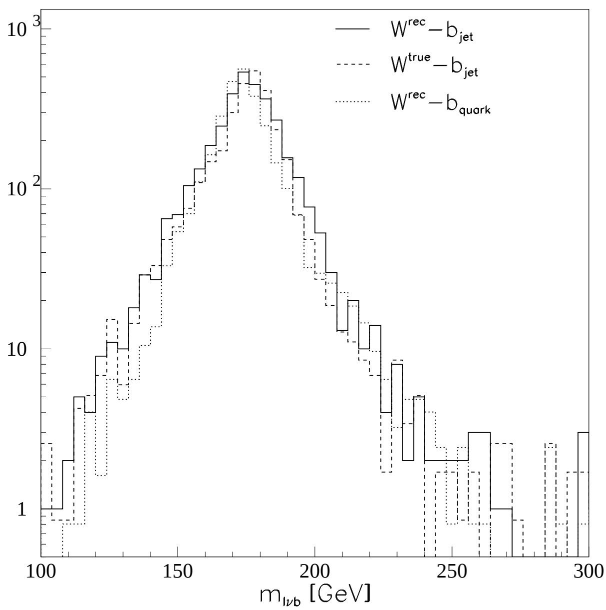

Fig. 5. Distribution of reconstructed top-quark mass, $m_{\ell\nu b}$, for $t \to \ell\nu b$ decays in inclusive $t\bar{t}$ events. The solid histogram corresponds to fully reconstructed $t \to \ell\nu b$ decays ($W^{\rm rec} + b_{\rm jet}$), the dashed one to partial reconstruction using the true W-boson ($W^{\rm true} + b_{\rm jet}$), and the dotted one to partial reconstruction using the true b-quark ($W^{\rm rec} + b_{\rm quark}$).

TABLE VII

Acceptances, mass resolutions and fractions of events in tails for fully reconstructed $t \to \ell\nu b$ decays as a function of the "quality" cuts applied to the $W \to \ell\nu$ reconstruction.

Selection	Acceptance	σ [GeV]	Fraction outside $\pm 2\sigma$
$\Delta \geq 0$	0.78	10.0 ± 0.4	16%
$R_{WW^{\rm rec}} < 1.0$	0.66	9.3 ± 0.2	15%
$R_{WW^{\rm rec}} < 0.5$	0.54	9.1 ± 0.3	14%
$R_{\nu\nu^{\rm rec}} < 1.0$	0.52	9.3 ± 0.2	14%
$R_{\nu\nu^{\rm rec}} < 0.5$	0.38	9.1 ± 0.3	13%
$p_x^\nu - p_x^{\nu{\rm rec}} < 3\sigma$	0.75	9.8 ± 0.2	13%
$p_z^\nu - p_z^{\nu{\rm rec}} < 3\sigma$	0.50	9.4 ± 0.3	14%

TABLE VIII

For fully reconstructed $t \to \ell\nu b$ decays, acceptances, ratios of events under the peak (R_p) and in the tails (R_t) before and after the "quality" cuts applied, and fraction of events outside the top-quark mass window as a function of the "quality" cuts applied to the reconstruction (see text).

Selection	Acceptance	R_p	R_t	$Acc * R_p/R_t$	Fraction outside ± 20 GeV
$\Delta \geq 0$	0.78	1.0	1.0	0.78	16%
$R_{WW^{\rm rec}} < 1.0$	0.66	0.77	0.68	0.75	15%
$R_{WW^{\rm rec}} < 0.5$	0.54	0.71	0.59	0.65	14%
$R_{\nu\nu^{\rm rec}} < 1.0$	0.52	0.69	0.63	0.57	14%
$R_{\nu\nu^{\rm rec}} < 0.5$	0.38	0.52	0.42	0.47	13%
$R_{tt^{\rm rec}} < 1.0$	0.61	0.78	0.75	0.63	15%
$R_{tt^{\rm rec}} < 0.5$	0.51	0.66	0.60	0.56	14%
$R_{WW^{\rm rec}} < 1.0$ $+R_{tt^{\rm rec}} < 1.0$	0.57	0.73	0.67	0.62	15%
$R_{WW^{\rm rec}} < 0.5$ $+R_{tt^{\rm rec}} < 0.5$	0.45	0.58	0.48	0.54	14%

3.2. Single top-quark reconstruction in the hadronic channel

3.2.1. $W \to jj$ reconstruction

To minimise the combinatorial background from jets originating from initial or final state QCD radiation only jets with a reconstructed transverse

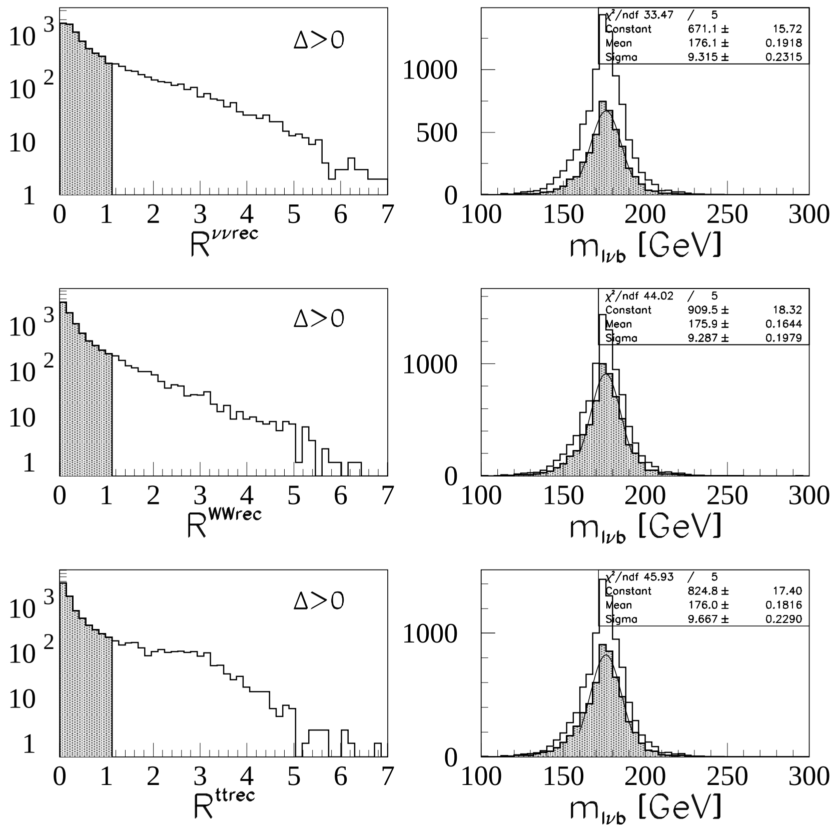

Fig. 6. Distribution of the differences between reconstructed and initial directions (left) and reconstructed mass (right) for $t \to \ell \nu b$ decays in inclusive $t\bar{t}$ events. The plots are shown for the neutrino (top), the W-boson (middle) and the top-quark (bottom).

energy $p_{\rm T}^{\rm jet} > 20$ GeV are considered for $W \to jj$ reconstruction. All possible pairs of such jets are considered and the distribution of their invariant mass m_{jj} is shown in Fig. 7 as a function of the ingredients used in the event generation. The signal from $W \to jj$ decays is clearly visible above the combinatorial background and the expected resolution increases from $\sigma_m = 5.3$ GeV (only hard scattering process) to $\sigma_m = 12.6$ GeV (initial and final state radiation and hadronisation/decays included).

The mass resolution improves with the increasing transverse momenta of the jj pair, $p_{\rm T}^{jj}$, as illustrated in Table IX. Only jj combinations with $m_{jj} = m_W \pm 25$ GeV ($\pm 2\sigma_m$ mass window) are retained for further analysis. In 76% of events at least one such combination is found as shown in Table IX.

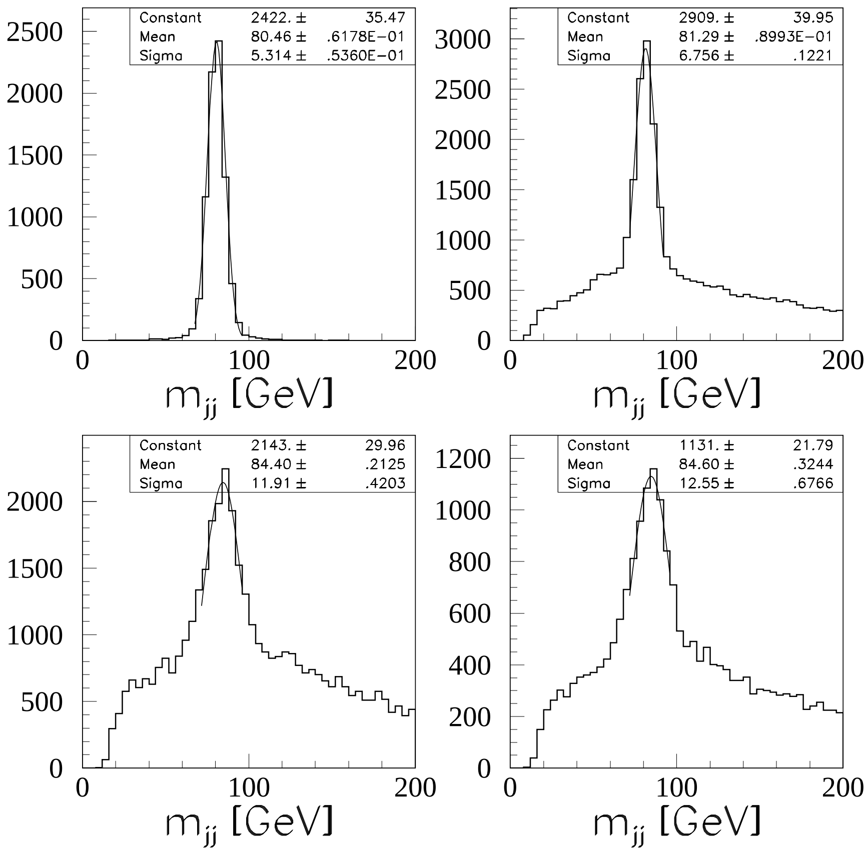

Fig. 7. Distribution of reconstructed invariant mass of jet pairs, m_{jj}, as a function of the ingredients used in the event generation: hard scattering process (top left), initial state radiation (top right), final state radiation (bottom left) and hadronisation/decays (bottom right).

TABLE IX

The expected acceptance for at least one jj combination in the chosen m_{jj} mass window (left side) and the resolution as the function of the transverse momenta of the jj pair (right side).

Mass window	Acceptance	p_{T}^{jj} [GeV]	$\sigma_{m_{jj}}$ [GeV]
± 15 GeV	65%	$50 - 100$	14.0
± 25 GeV	76%	$100 - 150$	10.5
± 30 GeV	80%	$150 - 200$	9.8

The resolution of the reconstructed m_{jj} would be better if the best combination, the one minimising $\chi^2 = (m_{jj} - m_W)^2$ was chosen. Fig. 8 shows reconstructed mass distribution for all combinations (left) and for the best combination (right). Resolution improves from $\sigma_m = 12.6$ GeV to $\sigma_m = 7.8$ GeV. However the best combination might not be the optimal one for the $t \to jjb$ reconstruction. The resolution of the reconstructed m_{jj} would also improve with increasing transverse momenta of jj pair, as illustrated in Table IX.

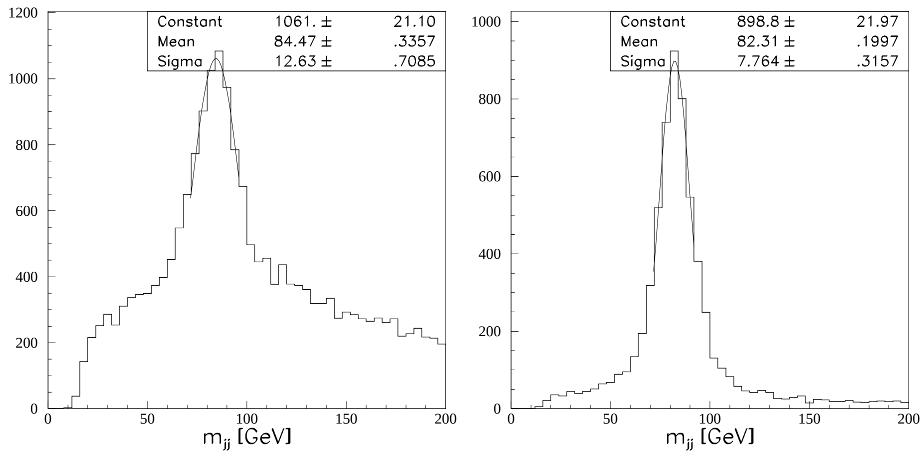

Fig. 8. Distribution of reconstructed invariant mass of jet pairs, m_{jj}, for all combinations (left) and for the best combination (right).

3.2.2. $t \to jjb$ reconstruction

For each $W \to jj$ candidate with $m_{jj} = 80 \pm 25$ GeV the jj four-momenta are rescaled to impose the constraint $m_{jj} = m_W$ and two possible jjb combinations are considered. Out of all possible jjb combinations the one which minimises the value of $\chi^2 = (m_{jjb} - m_t)^2$ is chosen. Figs 9 shows reconstructed invariant mass as a function of ingredients used for the event generation. The expected resolution increases from $\sigma_m = 6.2$ GeV (only hard scattering process) to $\sigma_m = 11.1$ GeV (initial and final state radiation and hadronisation/decays included) for the best combination of the jjb. The peak is almost Gaussian and well centred around m_t. The distribution of m_{jj} for all combinations (solid), best combination (dashed) and combinations selected as optimal one for the $t \to jjb$ reconstruction is shown on Fig. 10. As expected, mass resolution of the m_{jj} combinations chosen for $t \to jjb$ reconstruction is close to the resolution of the best jj combination for $W \to jj$ reconstruction.

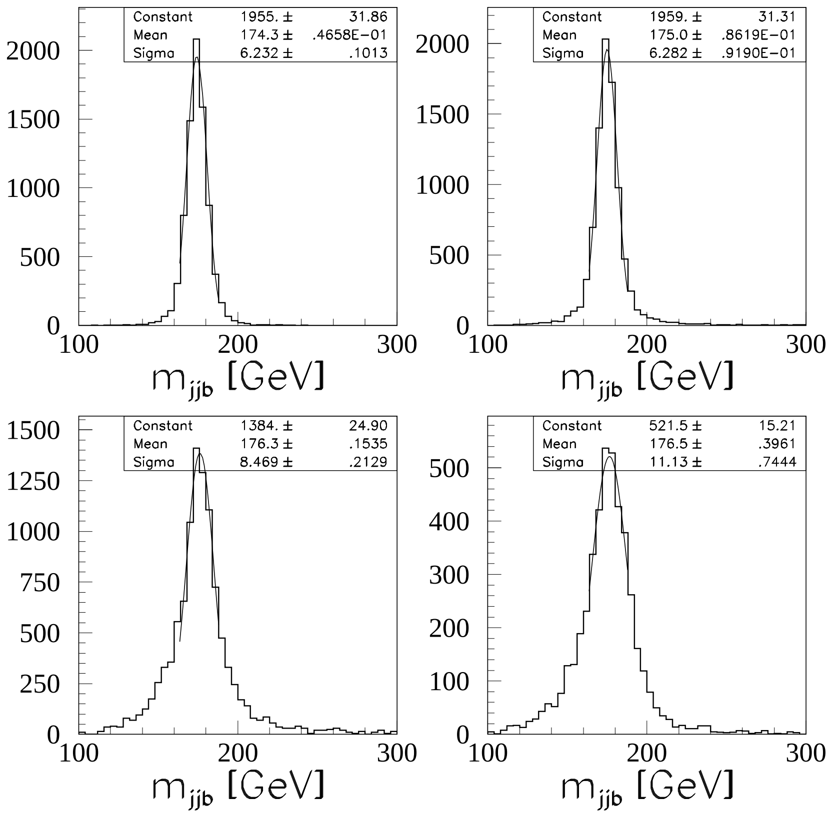

Fig. 9. Distribution of reconstructed invariant mass of $t \to jjb$, for best combination of jjb, as a function of the ingredients used in the event generation: hard scattering process (top left), initial state radiation (top right), final state radiation (bottom left) and hadronisation/decays (bottom right).

Similarly as for the semileptonic channel, full and partial reconstruction of $t \to jjb$ decays has been studied. The respective contributions to the mass resolution from the $W \to jj$ and b-jet reconstruction are illustrated in Fig. 11, which shows the m_{jjb} distributions in the case of the full and partial reconstruction of the $t \to jjb$ decay (see Section 3.1.2). The mass resolutions obtained and the fractions of events outside $\pm 2\sigma$ are given in Table X. The $t \to jjb$ resolution is dominated by the quality of the b-jet reconstruction, once the W-mass constraint has been applied to the reconstructed $W \to jj$ decay.

Taking as an initial selection for $t \to jjb$ decays the requirement $m_{jj} = 80 \pm 25$ GeV, one can study possible "quality" cuts for the top-quark re-

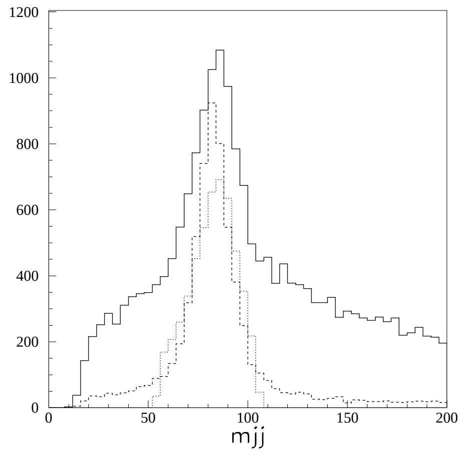

Fig. 10. Distribution of reconstructed invariant mass m_{jj} for all combinations (solid), best combination (dashed) and the combinations chosen as optimal ones for the $t \to jjb$ reconstruction (dotted).

TABLE X

Mass resolutions and fraction of events in tails for fully and partially reconstructed $t \to jjb$ decays in inclusive $t\bar{t}$ events (see text).

Selection	σ_m [GeV]	Fraction outside $\pm 2\sigma_m$	Fraction outside $\pm 2\sigma_1$
$W^{\rm rec} - b_{\rm jet}$	$11.1 \pm 0.7(\sigma_1)$	20%	20%
$W^{\rm true} - b_{\rm jet}$	8.7 ± 0.3	19%	13%
$W^{\rm rec} - b_{\rm quark}$	8.6 ± 0.4	20%	15%

construction. Tables XI and XII show example of such "quality" cuts as in Section 3.1.2. Although these quantities are not accessible experimentally, they can be used to quantify the fraction of "correct" and "false" top-quark reconstructions. The acceptance (Acc) of such "quality" cuts, the ratio of events passing such "quality" cuts to all events inside the chosen mass window of ± 20 GeV (R_p) and outside mass window (R_t), and the fraction of events outside the mass window are given in Table XII. In all cases, the fraction of events outside ± 20 GeV is around 20%. The highest quality reconstruction should maximise the value of $Acc \cdot R_p/R_t$; this value is found to be between 0.8 and 0.9 for "quality" cuts presented in Table XII. The best reconstruction should also be characterised by a large difference between the values of R_p and R_t; this difference is found to be between 0.17 and 0.27,

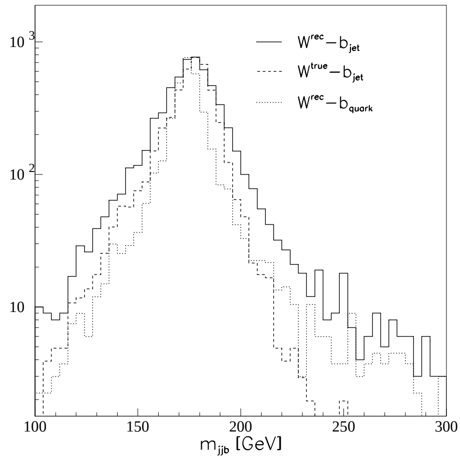

Fig. 11. Same as Fig. 5 for $t \to jjb$ channel

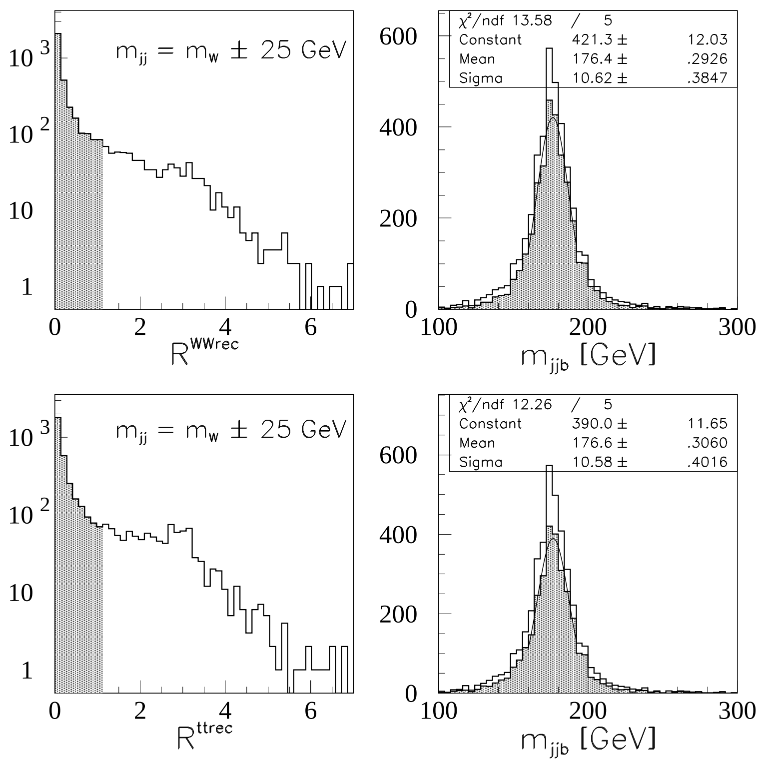

Fig. 12. Same as Fig. 6 for $t \to jjb$ decays.

much larger than in the $t \to \ell\nu b$ case. The m_{jjb} distributions before and after "quality" cuts on the $R^{W,W-\mathrm{rec}}$ and $R^{t,t-\mathrm{rec}}$ are shown in Fig. 12. The acceptance of these "quality" cuts is between 70 and 90% (see Table XII) which quantifies the fraction of correctly reconstructed $t \to jjb$ decays.

TABLE XI

Acceptance, mass resolutions and fractions of events in tails for fully reconstructed $t \to jjb$ decays as a function of the "quality" cuts applied to the reconstruction (see text).

Selection	Acceptance	σ [GeV]	Fraction outside $\pm 2\sigma$
$m_{jj} = 80 \pm 25$ GeV	0.76	11.1 ± 0.7	20%
$R_{WW^{\mathrm{rec}}} < 1.0$	0.64	10.6 ± 0.4	19%
$R_{WW^{\mathrm{rec}}} < 0.5$	0.55	10.4 ± 0.4	17%
$R_{tt^{\mathrm{rec}}} < 1.0$	0.60	10.6 ± 0.4	20%
$R_{tt^{\mathrm{rec}}} < 0.5$	0.51	10.4 ± 0.4	19%

TABLE XII

Same as Table VIII for $t \to jjb$ decays

Selection	Acceptance	R_p	R_t	$Acc * R_p/R_t$	Fraction outside ± 22 GeV
$m_{jj} = 80 \pm 25$GeV	0.76	1.0	1.0	0.76	20%
$R_{WW^{\mathrm{rec}}} < 1.0$	0.66	0.84	0.62	0.89	19%
$R_{WW^{\mathrm{rec}}} < 0.5$	0.58	0.76	0.49	0.90	17%
$R_{tt^{\mathrm{rec}}} < 1.0$	0.60	0.79	0.62	0.76	20%
$R_{tt^{\mathrm{rec}}} < 0.5$	0.55	0.70	0.50	0.77	19%
$R_{WW^{\mathrm{rec}}} < 1.0$ + $R_{tt^{\mathrm{rec}}} < 1.0$	0.58	0.74	0.53	0.81	18%
$R_{WW^{\mathrm{rec}}} < 0.5$ + $R_{tt^{\mathrm{rec}}} < 0.5$	0.50	0.65	0.40	0.81	17%

3.3. Reconstruction of top-quark pairs

The procedure for the reconstruction of both the $t \to \ell\nu b$ and $t \to jjb$ decays simultaneously chooses the best jjb and $l\nu b$ combinations, which therefore must minimise the value of

$$\chi^2 = (m_{\ell\nu b} - m_t)^2 + (m_{jjb} - m_t)^2 . \tag{2}$$

The $W \to \ell\nu$ and $W \to jj$ decays are reconstructed as described in the previous sections. All possible $l\nu b$ and jjb combinations are considered and the

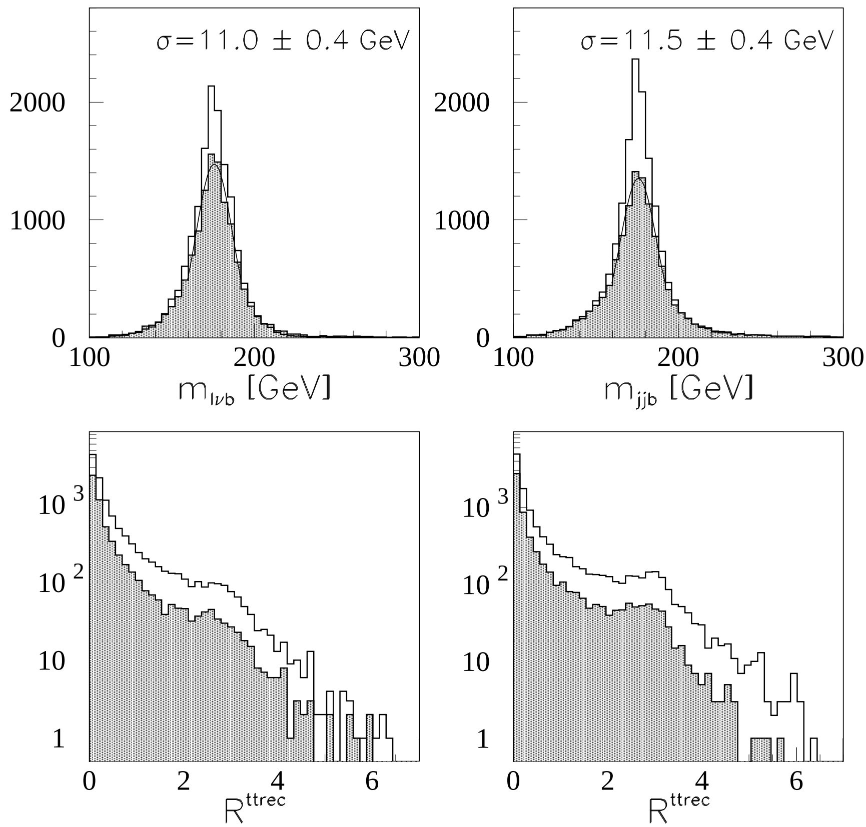

Fig. 13. Distributions of reconstructed top-quark masses, $m_{\ell\nu b}$ and m_{jjb}, in inclusive $t\bar{t}$ events for single top (solid histogram) and full $t\bar{t}$ (shaded histogram) reconstruction (top). Also shown (bottom) are the distributions of the distances between the reconstructed and initial top-quark directions, $R^{t,t-\mathrm{rec}}$.

best pair of such combinations is selected using Eq. (2). The quality of the reconstruction in terms of the distance $R^{t,t-\mathrm{rec}}$ is better in the case of the complete reconstruction of both top-quark decays than in the case of single reconstruction, as can be concluded from Fig. 13. Table XIII shows the acceptances of the selection criteria, the mass resolutions and the fractions of events outside the mass window for single top and full $t\bar{t}$ reconstruction and for a perfect b-tagging performance. Table XIV shows the same results for the b-tagging performance expected at low luminosity. However, obviously, both the acceptance and the mass resolution are somewhat worse if the reconstruction of both top-quarks is required. Only in 55% of events with one isolated lepton + 2 b-labelled reconstructed jets (perfect b-tagging) + 2 jets with deposited transverse energy above 20 GeV can the top-pair reconstruction algorithm can be applied (both $\Delta \geq 0$ and $m_{jj} = 80 \pm 25$ GeV), and in 61% of these events both $m_{\ell\nu b}$ and m_{jjb} are reconstructed inside the required mass window. This initial acceptance of 55% is degraded to 50% and the mass resolution increases slightly if the b-tagging performance at low luminosity is assumed (see Table XIV).

TABLE XIII

For single top and full $t\bar{t}$ reconstruction and for perfect b-tagging performance, acceptances, mass resolutions and fractions of events in tails.

Selection	Acceptance	σ [GeV]	Fraction inside $\pm 2\sigma$	Fraction outside $\pm 2\sigma$
Single $t \to l\nu b$				
$\Delta \geq 0$	0.78	10.0 $\pm$ 0.4	84%	16%
Single $t \to jjb$				
$m_{jj} = m_W \pm 25$GeV	0.76	11.0 $\pm$ 0.7	80%	20%
Both top quarks:	0.55		61%	
$t \to l\nu b$		11.0 $\pm$ 0.4	81%	19%
$t \to jjb$		11.5 $\pm$ 0.4	78%	22%

TABLE XIV

Same as Table XIII for the b-tagging performance expected at low luminosity.

Selection	Acceptance	σ [GeV]	Fraction inside $\pm 2\sigma$	Fraction outside $\pm 2\sigma$
Single$t \to l\nu b$				
$\Delta \geq\ 0$	0.73	10.6 $\pm$0.4	80 %	20%
Single $t \to jjb$				
$m_{jj} = m_W \pm 25$GeV	0.72	11.5 $\pm$0.4	78 %	22%
Both top quarks:	0.50		60%	
$t \to l\nu b$		12.5 $\pm$0.6	83%	17 %
$t \to jjb$		12.5 $\pm$0.6	76%	24 %

3.4. The high luminosity case

At high luminosity the detector performance in terms of $E_{\mathrm{T}}^{\mathrm{miss}}$ resolution, mass resolutions and b-tagging performance is degraded.

- With the fast simulation the obtained resolution of $E_{\mathrm{T}}^{\mathrm{miss}}$, $\sigma_{\mathrm{miss}} = 11.3$ GeV, represents rather ultimate performance of the detector (the pile-up is not added to empty cells). It is to be compared with the $\sigma_{\mathrm{miss}} = 5.7$ GeV expected at low luminosity.

- The jets energy threshold has to be raised to 30 GeV reducing the selection acceptance and the expected resolution is degraded both for the $t \to jjb$ and $t \to \ell\nu b$ reconstruction. For the $W \to jj$ reconstruction the m_{jj} peak is broader and pairs of jets from mass window ± 40 GeV are accepted for reconstruction of $t \to jjb$ channel.

- The expected b-tagging performance is degraded to $\varepsilon_b = 50\%$ for the same jets rejection.

- The thresholds on trigger lepton has to be raised respectively to 20 GeV for muons and 30 GeV for electrons.

The acceptance of the initial selection criteria is degraded by 30% due to the thresholds raised for leptons and jets transverse momenta while the acceptance of the reconstruction criteria alone changes only slightly. Table XV shows the acceptances of the reconstruction criteria, the mass resolutions and the fractions of events outside the mass window for single top and full $t\bar{t}$ reconstruction and for a perfect b-tagging performance. Table XVI shows the same results for the b-tagging performance expected at high luminosity. However, obviously, both the acceptance and the mass resolution are somewhat worse if the reconstruction of both top-quarks is required. Only 54% of events with passed initial selection (one trigger lepton + 2 b-labelled jets + 2 other jets) can be fully reconstructed (both $\Delta \geq 0$ and $m_{jj} = 80 \pm 40$ GeV), and in 62 % of these events both $m_{\ell\nu b}$ and m_{jjb} are reconstructed inside the required mass window. The acceptance of 54% is degraded to 48% of the initially selected events and the mass resolution increases slightly if the b-tagging performance at high luminosity is assumed (see Table XVI). Let us stress however that all numbers above present results from the fast simulation only and the efficiencies/acceptances of reconstruction procedures should be confirmed with the results from the full simulation of the ATLAS detector.

TABLE XV

Same as Table XIII for jets reconstruction performance expected at high luminosity (pile-up included and jets threshold increased to 30 GeV).

Selection	Acceptance	σ [GeV]	Fraction inside $\pm 2\sigma$	Fraction outside $\pm 2\sigma$
Single $t \to l\nu b$ $\Delta \geq 0$	0.71	11.2 $\pm$ 0.5	81%	19%
Single $t \to jjb$ $m_{jj} = 80 \pm 40$GeV	0.64	11.6 $\pm$ 0.5	81%	19%
Both top quarks:	0.54		62%	
$t \to l\nu b$		13.0 $\pm$ 0.5	84%	16%
$t \to jjb$		13.0 $\pm$ 0.5	80%	20%

TABLE XVI

Same as Table XV for the b-tagging performance expected at high luminosity.

Selection	Acceptance	σ [GeV]	Fraction inside $\pm 2\sigma$	Fraction outside $\pm 2\sigma$
Single $t \to l\nu b$	0.69	11.3$\pm$0.5	80%	20%
Single $t \to jjb$	0.60	12.0$\pm$0.5	80%	20%
Both top quarks:	0.48		59%	
$t \to l\nu b$		13.5$\pm$0.5	82%	18%
$t \to jjb$		13.5$\pm$0.5	78%	22%

4. Observability of the $t\bar{t}H$, $H \to b\bar{b}$ channel with full reconstruction of the final state

The full reconstruction of the final state for $t\bar{t}H$, $H \to b\bar{b}$ events requires $t\bar{t}$ reconstruction in the $t \to \ell\nu b$ and $t \to jjb$ channels and the reconstruction of the $H \to b\bar{b}$ peak.

The isolated trigger lepton and at least six reconstructed jets with $p_{\rm T} > 15$ GeV are required in the initial selection. The acceptance of these selection criteria is 56% for the signal events with m_H=100 GeV and one $W \to \ell\nu$ and $H \to b\bar{b}$ decays. Four of these jets are required to be tagged as b-jets.

The reconstruction of the top-quark pair is optimised as discussed in Section 3.3. Fig. 14 shows the expected m_{jjb} and $m_{\ell\nu b}$ and $R^{t,t-{\rm rec}}$ distributions for the top-quark pair reconstruction in the $t\bar{t}H$ events for the low-luminosity

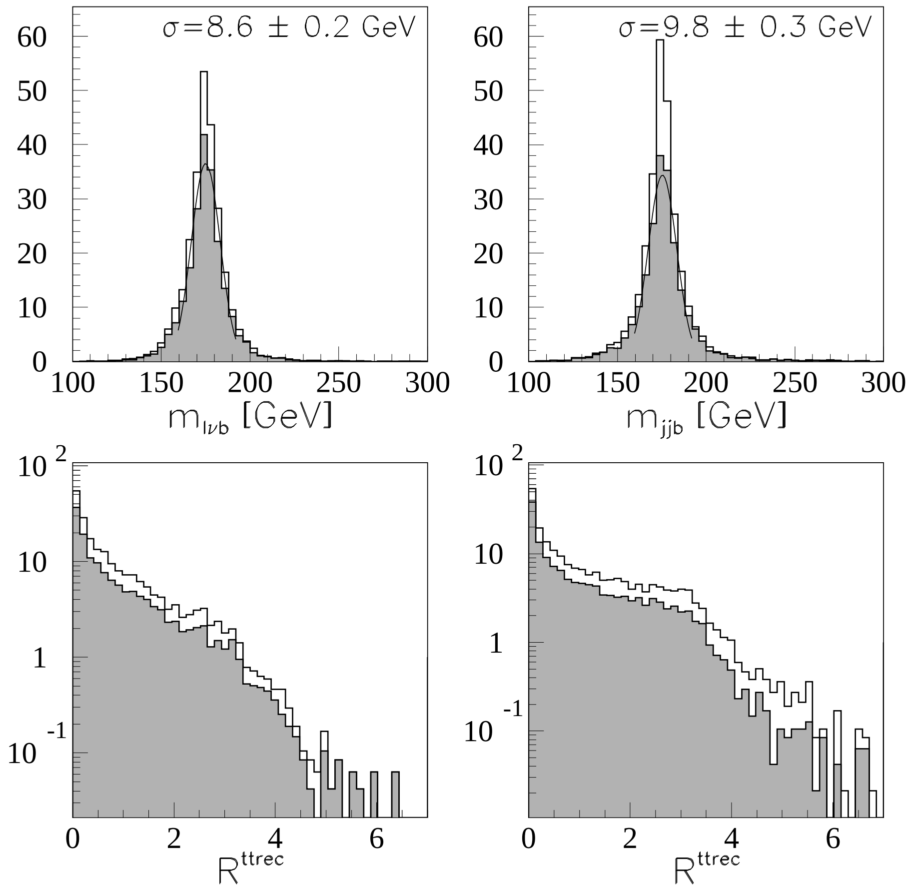

Fig. 14. Distribution of reconstructed top-quark masses, $m_{\ell\nu b}$(top left) and m_{jjb}(top right) for $t\bar{t}H$ events with m_H=100 GeV and for the b-tagging performance expected at low luminosity. Also shown (bottom) are the distributions of the distances between the reconstructed and initial top-quark directions. The plots are shown for single top reconstruction (solid histograms) and for the reconstruction of both top quarks (shaded histograms).

b-tagging performance. The mass resolution obtained is better than in simpler $t\bar{t}$ case as can be seen by comparing Table XIV and XVIII, because the average transverse momenta of the top-quarks in $t\bar{t}H$ events are higher than in inclusive $t\bar{t}$ events. The mass spectrum of remaining two b-jets, not chosen for the top-pair reconstruction, is peaked around m_{bb}=100 GeV, as shown on Figs 15 and 16.

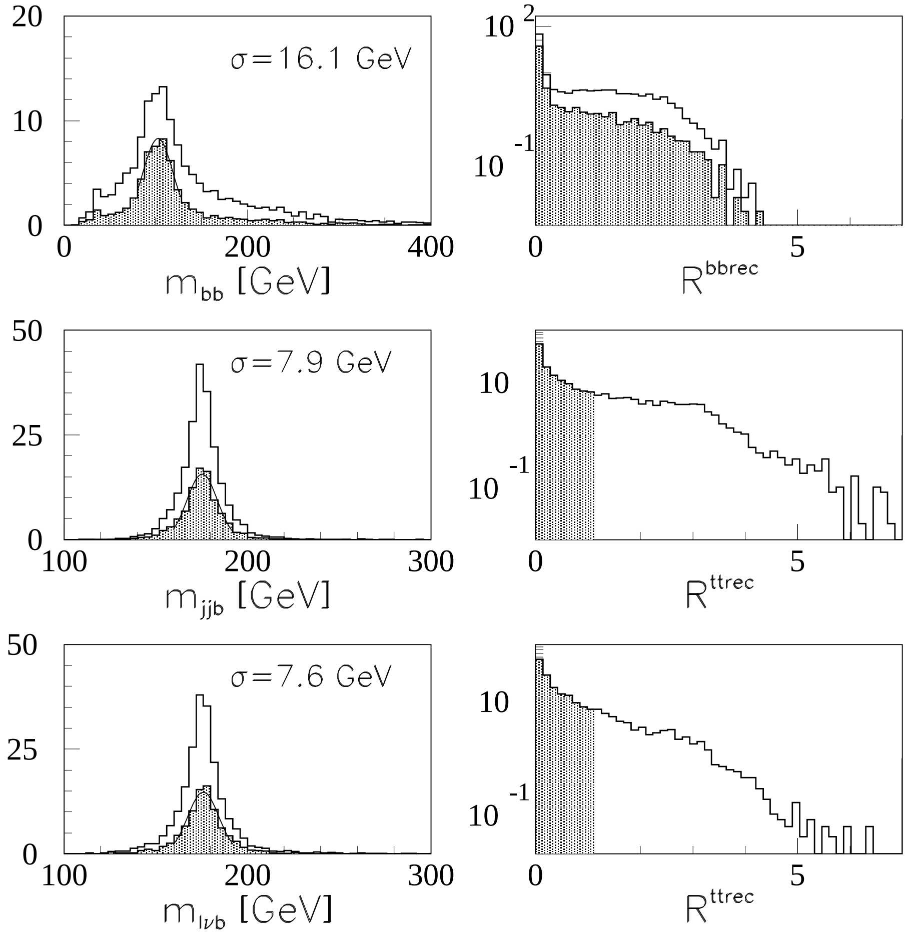

Fig. 15. For fully reconstructed $t\bar{t}H$, $H \to b\bar{b}$ events and for the low luminosity b-tagging performance, distributions of the reconstructed masses, m_{bb}, m_{jjb} and $m_{\ell\nu b}$, and of the distances $R^{b,b-\mathrm{rec}}$ and $R^{t,t-\mathrm{rec}}$. The results are shown for all events (solid histogram) and for events with $R^{t,t-\mathrm{rec}} < 1.0$ for both top-quark decays (shaded histogram).

The expected numbers of signal and background events at each consecutive step of the reconstruction procedure[3] are given in Table XVII. As discussed in Section 2 the main background comes from $t\bar{t}jj$ which is dominated, about 56%, by the true $t\bar{t}bb$ events and not negligible fraction of $t\bar{t}cc$ events. This background is efficiently suppressed with presented above

[3] Mass window of ±20 GeV,±20 GeV and ±30 GeV are used for the $t \to \ell\nu b$, $t \to jjb$ and $H \to b\bar{b}$ reconstruction respectively.

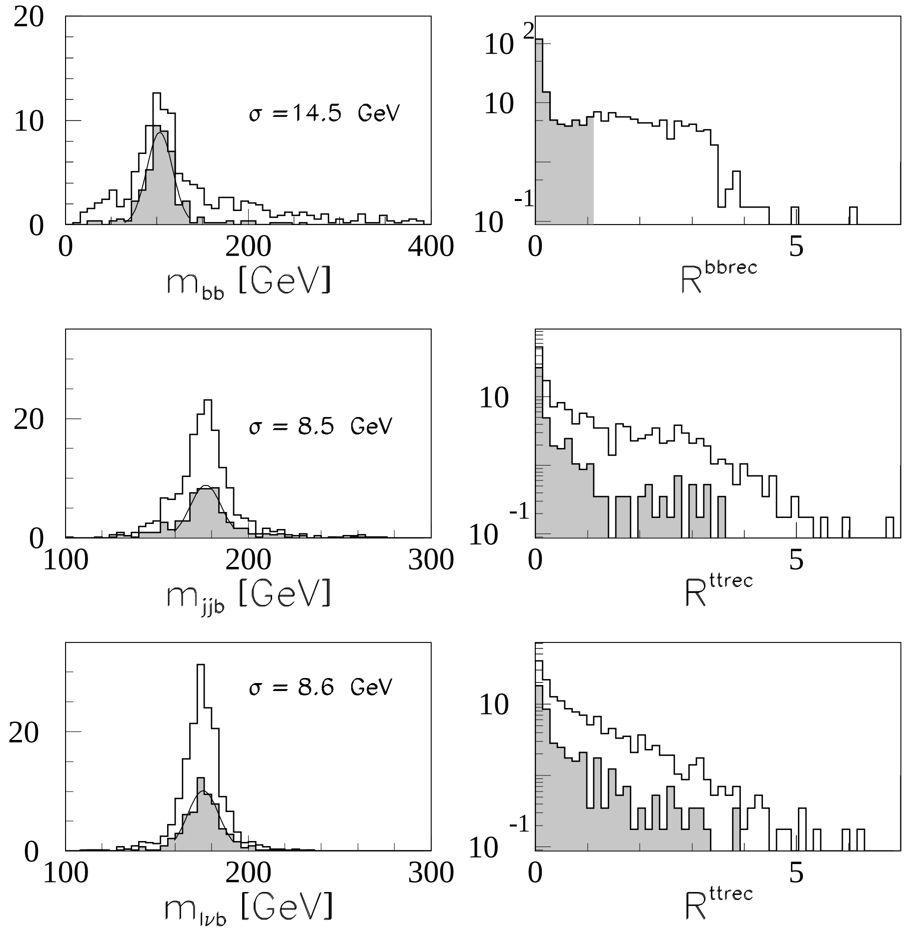

Fig. 16. Same as Fig. 15 but for $R^{b,b-\mathrm{rec}} < 1.0$ (shaded histogram).

procedure as compared to the more inclusive reconstruction discussed in Section 2. The acceptances in the mass window and the fractions of events inside and outside the mass window are given in Tables XVIII and XIX for the b-tagging performance expected at low luminosity. As discussed in Section 2 an increase of the mass window for m_{bb}, *e.g.* from $\pm\ 1.5\sigma_m$ to $\pm\ 2\sigma_m$, improves slightly the signal–to–background ratio and the statistical significance, but reduces the purity of the $H \to b\bar{b}$ signal in the m_{bb} peak, owing to the larger combinatorial background from the signal events themselves and therefore reduces $\mathrm{S}_{H\to b\bar{b}}/\mathrm{S}_{\mathrm{total}}$.

TABLE XVII

Expected numbers of signal and background events at each consecutive step of the reconstruction procedure for $t\bar{t}H$, $H \to b\bar{b}$ events with m_H=100 GeV and for an integrated luminosity of $3 \cdot 10^4$ pb^{-1}.

Process	6 jets in $\lvert\eta\rvert < 5.0$ + one isol. lepton	+4 tagged b-jets	+ $m_{jjb}, m_{l\nu b}$ in mass window	$+m_{bb}$ in mass window
$t\bar{t}H$	5900	365	140	61
$t\bar{t}$ + jets in $p_{\mathrm{T}}^{\mathrm{hard}}$ bins				
1–20 GeV	9700	35	10	5
20–50 GeV	49600	155	50	10
50–100 GeV	155400	510	85	25
100–150 GeV	168700	560	130	35
150–200 GeV	122200	380	100	30
> 200 GeV	159500	620	150	25
Total ($t\bar{t}$ + jets)	665100	2260	525	130
W + jets in $p_{\mathrm{T}}^{\mathrm{hard}}$ bins				
1–20 GeV	31100	22	8	4
20–50 GeV	38400	10	2	—
50–100 GeV	59100	10	3	2
100–150 GeV	39600	3	1	1
150–200 GeV	21900	3	1	1
> 200 GeV	10000	2	—	—
Total (W + jets)	200100	50	14	8

For fully reconstructed signal events, "quality" cuts such as $R^{b,b-\mathrm{rec}} < 1.0$ and $R^{t,t-\mathrm{rec}} < 1.0$ on the distances between the reconstructed and initial b-jets from $H \to b\bar{b}$ decay and between the reconstructed and initial top-quark directions can be applied to study the quality of the reconstruction, as illustrated in Tables XVIII–XIX. Clearly, an increased purity of the top-quark reconstruction ($R_{t,t-\mathrm{rec}} < 1.0$) improves the $H \to b\bar{b}$ reconstruction (both the m_{bb} resolution and the acceptance in the mass window). Consistently, an increased purity of the $H \to b\bar{b}$ reconstruction ($R_{b,b-\mathrm{rec}} < 1.0$) improves the quality of the top-quark reconstruction. These effects are also illustrated in Figs. 15 and 16.

For the $t\bar{t}$+jets background events, the reconstructed distributions of $m_{\ell\nu b}$, m_{jjb} and m_{bb} have different features. Quality cuts such as $R^{t,t-\mathrm{rec}} < 1$ obviously improve the top-quark reconstruction but have no effect on the m_{bb} distribution as can be seen in Fig. 17.

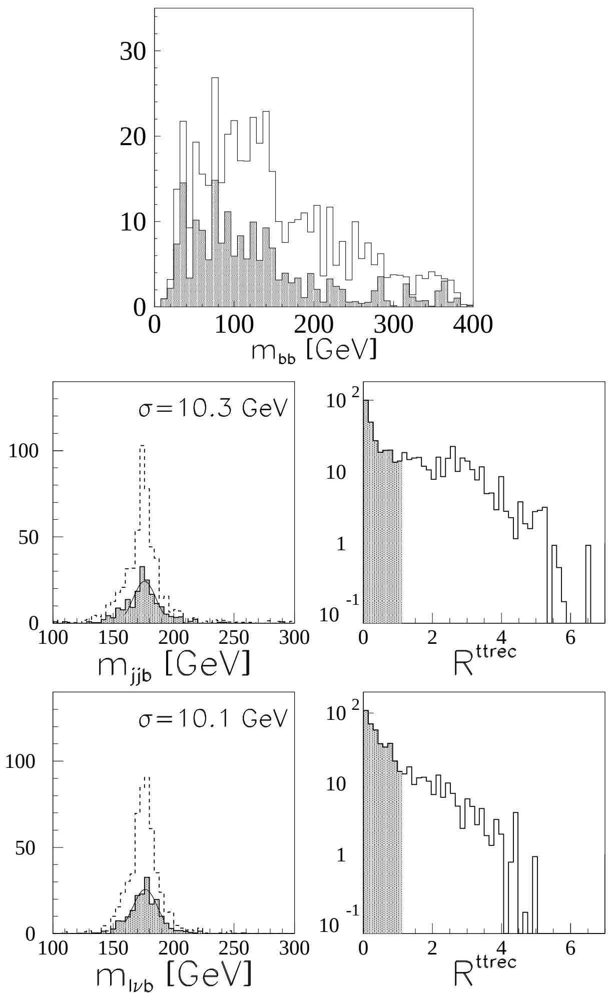

Fig. 17. For fully reconstructed $t\bar{t}$+jets background events and for the low luminosity b-tagging performance, distributions of the reconstructed masses, m_{bb}, m_{jjb} and $m_{\ell\nu b}$ and of the distance $R^{t,t-\mathrm{rec}}$. The results are shown for all events (solid histogram) and for events with $R^{t,t-\mathrm{rec}}$ < 1.0 for both top-quark decays (shaded histogram).

Although this "quality" cuts cannot be applied experimentally, they confirm the presence of correctly reconstructed $t \to Wb$ decays in the signal and background events and of correctly reconstructed $H \to b\bar{b}$ decays in the signal itself. They also confirm that the observed mass peaks are not an artefact of the selection procedure. This check is important since, as shown in Tables XX–XXI, only $\sim 60\%$ of the $H \to b\bar{b}$ decays in fully reconstructed

TABLE XVIII

For single top and top-quark pair reconstruction in $t\bar{t}H$ events for the b-tagging performance expected at low luminosity, acceptances, mass resolutions and fractions of events inside and outside $\pm 2\sigma_{m_t}$.

Selection	Acceptance	σ_{m_t} [GeV]	Fraction inside $\pm 2\sigma_{m_t}$	Fraction outside $\pm 2\sigma_{m_t}$
Single$t \to l\nu b$	0.75	8.0±0.2	83%	17%
Single $t \to jjb$	0.80	7.5±0.2	80%	20%
Both top quarks:			0.60	
$t \to l\nu b$	0.60	8.6±0.2	83%	17%
$t \to jjb$		9.8±0.3	78%	22%
Both with $R_{t,t-\mathrm{rec}} < 1.0$:	0.26			
$t \to l\nu b$		7.6±0.3	83%	17%
$t \to jjb$		7.9±0.4	80%	20%

TABLE XIX

For $H \to b\bar{b}$ reconstruction in $t\bar{t}H$ events and for the b-tagging performance expected at low luminosity, acceptance, mass resolution and fraction of events inside and outside $\pm 2\sigma_{m_{bb}}$ as a function of the "quality" cuts chosen.

Selection	Acceptance	$\sigma_{m_{bb}}$ [GeV]	Fraction inside $\pm 2\sigma_{m_{bb}}$	Fraction outside $\pm 2\sigma_{m_{bb}}$
b-jets matching for $t \to Wb$	1.0	20.0±1.5	45%	55%
both $t \to Wb$ in mass window	0.68	19.0±1.5	48%	52%
both $t \to Wb$ in mass window $R_{t,t-\mathrm{rec}} < 1.0$	0.31	16.1±0.5	66%	34%
both $t \to Wb$ in mass window $R_{b,b-\mathrm{rec}} < 1.0$	0.34	14.5±0.5	71%	29%

$t\bar{t}H$ events are reconstructed in the chosen mass window. Even though this represents an improvement of about a factor 2 with respect to the results of [2], the purity for reconstruction remains low because of the combinatorial problems due to the large number of jets in the final state.

The expected numbers of signal and background events with a fully reconstructed $t\bar{t}H$, $H \to b\bar{b}$ final state are given in Table XX for an integrated luminosity of $3 \cdot 10^4$ pb^{-1} and $m_H = 100$ GeV as a function of the b-tagging performance as taken from the Inner detector TDR [8]. The expected observability of this channel depends strongly both on the b-tagging efficiency and on the expected rejection of c-jets. Table XXI shows the expected signal and background rates for three different values of the Higgs-boson mass and for the low-luminosity b-tagging performance. As already observed in case of more inclusive analysis discussed in Section 2, for a narrower mass window the purity of the $H \to b\bar{b}$ reconstruction would be higher, while, for the wider one chosen the significance is better. For a Higgs-boson mass of 100 GeV and an integrated luminosity of $3 \cdot 10^4$ pb^{-1}, significance of 5.0σ is expected for the low-luminosity b-tagging performance with a signal-to-background ratio of 0.41 and a signal purity of 60%. This situation is much improved with respect to that described in [2] and in Section 2.

TABLE XX

Expected numbers of signal (S) and background (B) events, and significances for an integrated luminosity of $3 \cdot 10^4$ pb^{-1} for $m_H = 100$ GeV and mass window $m_{bb} = m_H \pm 30$ GeV, and for various b-tagging efficiencies and rejections using events with two reconstructed top-quarks (see text).

ε_b %	60	43	53	64.0	62.4
ε_j %	1.0	0.46	1.1	3.1	1.1
ε_c %	10.0	9.2	14.9	23.8	14.9
$t\bar{t}H$ (total S)	61	31	50	82	71
$t\bar{t}Z$	8	2	6	10	10
$Wjjjj$	12	2	10	20	10
$ttjj$	130	60	160	540	240
Total B	150	64	176	570	260
S/B	0.41	0.48	0.28	0.14	0.27
$\mathrm{S}/\sqrt{\mathrm{B}}$	5.0	3.9	3.8	3.4	4.4
$\mathrm{S}_{H\to b\bar{b}}/\mathrm{S}_{\mathrm{total}}$	0.64	0.63	0.57	0.54	0.59

Fig. 18 shows the expected summed signal+background distributions for $m_{\ell\nu b}$, m_{jjb} and for the low-luminosity b-tagging performance. The dark shaded histograms denote events for which both the $t \to \ell\nu b$ and $t \to jjb$ decays are reconstructed inside the chosen mass window. Fig. 19 shows the expected summed signal+background distributions for m_{bb} and for

TABLE XXI

Same as Table XX for the low-luminosity b-tagging performance and for three different values of the Higgs-boson mass.

	m_H=80 GeV	m_H=100 GeV	m_H=120 GeV
$t\bar{t}H$ (total S)	81	61	40
$t\bar{t}Z$	7	8	2
$Wjjjj$	17	12	5
$t\bar{t}jj$	121	130	120
Total B	145	150	127
S/B	0.56	0.41	0.32
$S/\sqrt{B}$	6.7	5.0	3.6
$S_{H\to b\bar{b}}/S_{\rm total}$	0.67	0.64	0.59

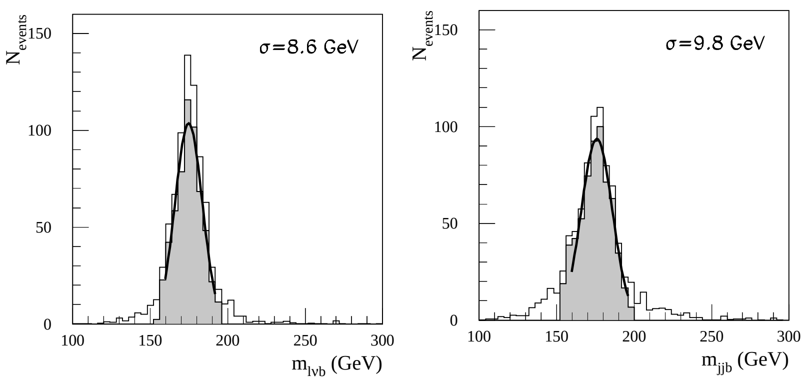

Fig. 18. Expected $m_{\ell\nu b}$, m_{jjb} distributions for the summed signal+background events and for an integrated luminosity of $3 \cdot 10^4$ pb^{-1}. The shaded histogram denotes events for which both top-quarks are reconstructed inside the chosen mass window.

m_H=100 GeV (left) and m_H=120 GeV (right) for events for which both the $t \to \ell\nu b$ and $t \to jjb$ decays are reconstructed inside the chosen mass window. The solid histogram shows the summed signal+background distribution, the light shaded histogram shows the background events alone while the dark shaded one shows the contribution from $H \to b\bar{b}$ decays. A clean peak is visible above the background shape which was not the case of the earlier more inclusive procedures (compare *e.g.* with the distributions in Fig. 3).

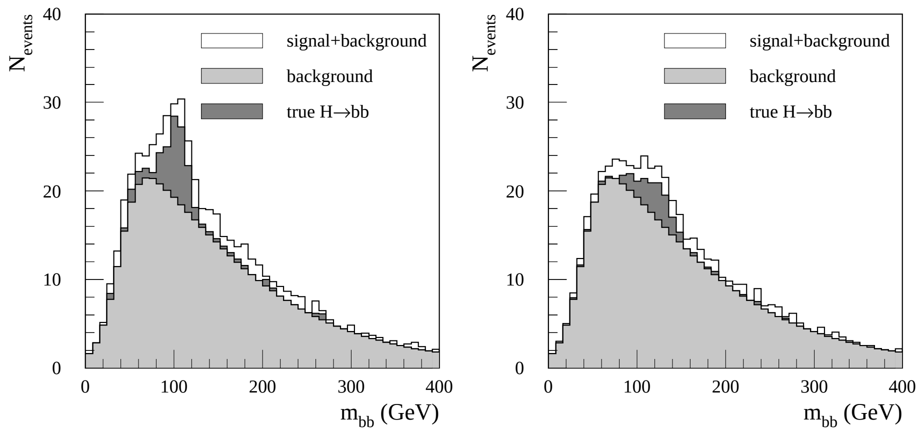

Fig. 19. Expected m_{bb} distributions for the summed signal+background events and for an integrated luminosity of $3 \cdot 10^4$ pb^{-1}and for $m_H = 100$ GeV (left) and 120 GeV (right). The solid histogram denotes signal+background events for which both top-quarks are reconstructed inside the chosen mass window, while the light shaded histogram shows the background events and the dark shaded denotes true $H \to b\bar{b}$ decays.

4.1. The high luminosity case

At high luminosity thresholds on the transverse energy of trigger lepton and of reconstructed jets has to be raised and the mass resolution for the m_{bb} reconstruction is degraded from $\sigma_m = 19$ GeV to $\sigma_m = 22$ GeV, with somewhat reduced acceptance, whereas the low-luminosity b-tagging efficiency is expected to be reduced to $\varepsilon_b = 50\%$ for the same jet rejection. The acceptance of the initial kinematical cuts (higher transverse energy thresholds for trigger lepton and reconstructed jets) is reduced by 7 % for the signal events themselves, but the purity of the reconstruction remains more or less constant. As for the low-luminosity case an increase of the mass window for m_{bb}, *e.g.* from $\pm\ 1.5\sigma_m$ to $\pm\ 2\sigma_m$, improves slightly the signal–to–background ratio and the statistical significance, but reduces the purity of the $H \to b\bar{b}$ signal in the m_{bb} peak, owing to the larger combinatorial background from the signal events themselves and therefore reduces $\mathrm{S}_{H\to b\bar{b}}/\mathrm{S}_{\mathrm{total}}$.

The expected numbers of signal and background events for an integrated luminosity of $3 \cdot 10^5$ pb^{-1} are given in Table XXIV. A 5σ significance for an integrated luminosity of $3 \cdot 10^5$ pb^{-1} is reached for the Higgs-boson masses somewhat higher than m_H=120 GeV. Fig. 20 shows the expected summed signal+background distributions for m_{bb} and for m_H=100 GeV for events for which both the $t \to \ell\nu b$ and $t \to jjb$ decays are reconstructed inside the chosen mass window. The solid histogram shows the summed sig-

TABLE XXII

Same as Table XVIII for the b-tagging performance expected at high luminosity.

Selection	Acceptance	σ_{m_t} [GeV]	Fraction inside $\pm 2\sigma_{m_t}$	Fraction outside $\pm 2\sigma_{m_t}$
Single$t \to l\nu b$	0.73	8.0±0.4	83%	17%
Single $t \to jjb$	0.83	7.8±0.3	79%	21%
Both top quarks:	0.60		0.66	
$t \to l\nu b$		9.0±0.4	83%	17%
$t \to jjb$		10.0±0.4	77%	23%
Both with $R_{t,t-\mathrm{rec}} < 1.0$:	0.26			
$t \to l\nu b$		8.8±0.6	84%	16%
$t \to jjb$		8.9±0.7	77%	23%

TABLE XXIII

Same as Table XIX for the b-tagging performance expected at high luminosity.

Selection	Acceptance	$\sigma_{m_{bb}}$ [GeV]	Fraction inside $\pm 2\sigma_{m_{bb}}$	Fraction outside $\pm 2\sigma_{m_{bb}}$
b-jets matching for $t \to Wb$	1.0	22.0±0.6	45%	55%
both $t \to Wb$ in mass window	0.60	22.0±0.6	50%	50%
both $t \to Wb$ in mass window $R_{t,t-\mathrm{rec}} < 1.0$	0.27	20.0±0.8	75%	25%
both $t \to Wb$ in mass window $R_{b,b-\mathrm{rec}} < 1.0$	0.25	18.0±0.5	82%	18%

nal+background distribution, the light shaded histogram shows the background events alone while the dark shaded one shows the contribution from $H \to b\bar{b}$ decays. The background shape is slightly kinematically shifted to higher values of the m_{bb} in respect to the low luminosity reconstruction as higher transverse momenta of reconstructed jets are required in multi-jet final state. The expected peak in the background distribution overlaps with the resonant peak from Higgs of 100 GeV mass just giving a bit less clear signature for the signal itself than it is expected for the low luminosity case.

TABLE XXIV

Same as Table XX for an integrated luminosity of $3 \cdot 10^5$ pb^{-1}, a mass window $m_{bb} = m_H \pm 45$ GeV, the high luminosity b-tagging performance and three different values of the Higgs-boson masses.

	m_H=80 GeV	m_H=100 GeV	m_H=120 GeV
$t\bar{t}H$(total S)	420	320	185
$t\bar{t}Z$	40	40	15
$Wjjjj$	105	45	30
$t\bar{t}$jj	740	750	726
Total B	885	835	771
S/B	0.43	0.38	0.24
S/$\sqrt{\text{B}}$	14.1	11.1	6.7
$\text{S}_{H\to b\bar{b}}/\text{S}_{\text{total}}$	0.57	0.53	0.50

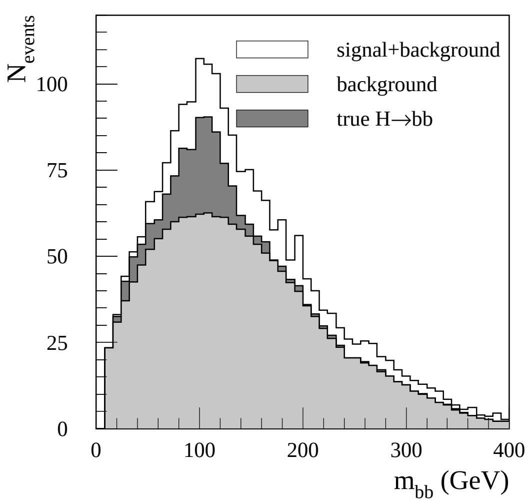

Fig. 20. The same as Fig. 19 but for Higgs mass of 100 GeV and for an integrated luminosity of $3 \cdot 10^5$ pb^{-1}.

5. Observability of the $t\bar{t}h$ with $h \to b\bar{b}$ channel in the MSSM Higgs sector

The $t\bar{t}h$/ Wh with $h \to b\bar{b}$ are very interesting but challenging for Higgs searches in the MSSM model. Both the production and the decay processes are described by tree-level Feynman diagrams, so they do not suffer from any potential suppression factors due to SUSY particles exchanged in virtual loops. Such suppression factors might deteriorate the sensitivity to the $h \to \gamma\gamma$ decay mode for *e.g.* light stop scenarios, if this channel is explored in the loop-mediated gluon-gluon fusion production process, or, more generally, in light χ_1^0 scenarios.

The experimental observability of the h-boson in the MSSM model with $h \to b\bar{b}$ in ATLAS has been discussed in [7] where the so-called 5σ-discovery contour in the $(m_A,\, \tan\beta)$ plane was drawn only for the Wh, $h \to b\bar{b}$ channel. The potential for the $t\bar{t}H$, $H \to b\bar{b}$ channel studied in [2] was rather unconvincing in terms of signal-to-background ratio and background shape. It was already suggested, however, that the complete reconstruction of the top-quark decays in this channel would most likely improve the situation sufficiently to provide good sensitivity in the MSSM Higgs sector.

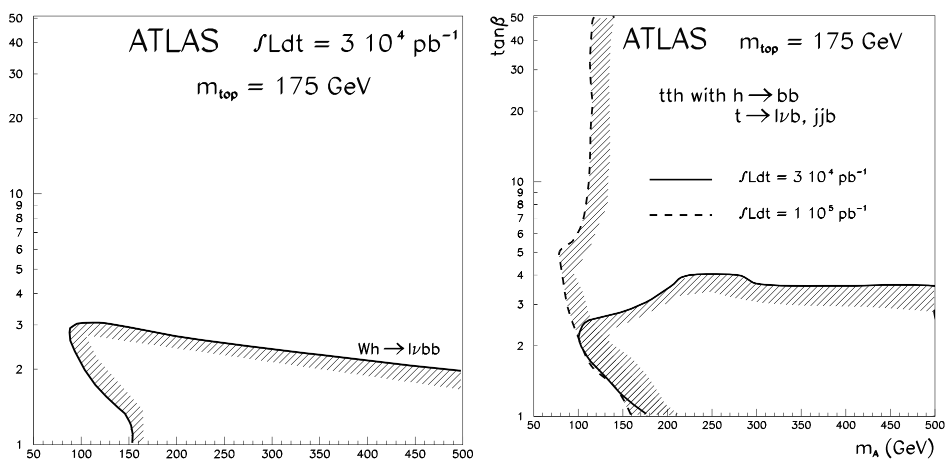

Fig. 21. In the $(m_A,\, \tan\beta)$ plane describing the MSSM Higgs sector, the 5σ-discovery contour curves for the Wh(left) and $t\bar{t}h$(right) with $h \to b\bar{b}$ channels, for integrated luminosities of $3 \cdot 10^4$ pb^{-1}(Wh and $t\bar{t}h$) and 10^5 pb^{-1}($t\bar{t}h$).

The results shown in the previous Section for the SM Higgs search in the $t\bar{t}H$, $H \to b\bar{b}$ channel with full final-state reconstruction are in fact very promising. In the MSSM case, the rates are even somewhat enhanced with respect to the SM case, as discussed in Section 3.1 of [7]. As shown in Fig 21, a large fraction of the $(m_A,\, \tan\beta)$ parameter space can already be covered with the $t\bar{t}h$ channel for an integrated luminosity of $3 \cdot 10^4$ pb^{-1}. For an integrated luminosity of 10^5 pb^{-1}, this channel alone would lead to h-boson discovery over most of the parameter space. Fig. 21 also shows for comparison the discovery potential for the Wh with $h \to b\bar{b}$ channel. The $t\bar{t}h$ channel provides better sensitivity particularly since it can readily be also explored at high luminosity (no strict jet-veto cuts needed to reject the background as in the Wh channel).

The above results are obtained with the assumption, as in [7], that SUSY particles are heavy (~ 1 TeV). It should be stressed however, that the observability of this channel will not be affected by the exact SUSY scenario, provided that the h-boson decay mode to the LSP is kinematically forbidden ($m_{\chi_1^0} > m_h/2$ GeV).

6. Conclusions

In this note the expected potential of the ATLAS detector at LHC for discovering a SM or MSSM Higgs boson in the $t\bar{t}H$, $H \to b\bar{b}$ channel has been discussed.

For the SM search, this channel is interesting in the narrow but difficult mass range above the LEP2 discovery limit and below 120–130 GeV. Requiring four b-tagged jets and a fully reconstructed final state, a signal significance above 5σ should be reached for an integrated luminosity of $3 \cdot 10^4$ pb^{-1} and for m_H below 100 GeV. For an integrated luminosity of 10^5 pb^{-1} the 5σ sensitivity range extends to $m_H \sim 120$ GeV and overlaps well with the region where the $H \to \gamma\gamma$ channel is accessible.

For the MSSM Higgs search and for an integrated luminosity of 10^5 pb^{-1} this channel covers a very large fraction of the (m_A, $\tan\beta$) parameter space. In particular this channel covers the small hole in the MSSM Higgs discovery potential expected so far for the ATLAS experiment even after collecting an integrated luminosity of $3 \cdot 10^5$ pb^{-1} [7].

Provided that light Higgs boson decays to SUSY particles are kinematically forbidden, the sensitivity to this channel cannot be degraded by other SUSY particles (no loops present neither in the production nor in the decay process). However, discovery in this channel alone would not allow to disentangle between the SM and MSSM Higgs scenarios.

Finally this channel will be accessible only if excellent b-tagging performance is achieved by the ATLAS detector. A better understanding of the potential of this channel requires more detailed simulations of the expected detector performance both in terms of the multi-jet reconstruction and of the b-tagging performance (especially at high luminosity).

The idea of exploring the full reconstruction of the final state in this channel is originates from D. Froidevaux to whom authors are greatly indebted as well as for many valuable comments and suggestions on this study.

REFERENCES

[1] J. Dai, J.F. Gunion, R. Vega, *Phys. Rev. Lett.* **71**, 2699 (1993).

[2] D. Froidevaux, E. Richter-Was, ATLAS Internal Note, PHYS-No-043 (1996); CERN preprint TH-7459/94; *Z. Phys.* **C67**, 213 (1995).

[3] E. Richter-Was, D. Froidevaux, ATLAS Internal Note, PHYS-No-104 (1997); CERN-preprint CERN-TH/210-97; *Z. Phys.* **C76**, 665 (1997).

[4] M. Cobal, D. Costanzo, S. Lami, ATLAS Internal Note, PHYS-No-084 (1996).

[5] E. Richter-Was, D. Froidevaux, L. Poggioli, ATLAS Internal Note, PHYS-No-079 (1996); for an updated version, see http://wwwcn.cern.ch/ erichter/Atlfast.html.

[6] T. Sjostrand, *Comput. Phys. Commun.* **82**, 74 (1994).

[7] E. Richter-Was *et al.*, ATLAS Internal Note, PHYS-No-074 (1996).

[8] ATLAS Collaboration, ATLAS Inner Detector TDR, CERN/LHCC/97-16; ATLAS TDR 4, 30 April 1997.